TABLE OF CONTENTS

Page

INTRODUCTION 1

CHAPTER 1 BACKGROUND 5
1.1 Facility Description 5
1.2 Uncertainty Analysis Overview 6
1.3 Review of the Literature 12
1.4 Objectives 17

CHAPTER 2 METHODOLOGY 19
2.1 Analysis Fundamentals 19
2.2 Data Reduction 21
2.3 Elemental Errors 25
2.4 Implementation 28

CHAPTER 3 RESULTS 33
3.1 Overall Uncertainty Estimates 33
3.2 Uncertainty Breakdowns 43
3.3 Validation 55

CONCLUSION 69

APPENDIX I THE NRC TRISONIC FACILITY 73

APPENDIX II THE HALF-MODEL BALANCE 75

LIST OF REFERENCES 77

LIST OF TABLES

Page

Table 1.1 Common nominal test conditions of Bombardier half-model experiments 6

Table 2.1 Estimates of the bias and precision limits of the independent variables 26

LIST OF FIGURES

Page

Figure 0.1 A Bombardier half-model installed in the 1.5 by 1.5 m transonic test section of the NRC wind tunnel 3

Figure 1.1 Effect of errors in a sample of successive measurements of a variable 7

Figure 2.1 Location of the balance force components relative to the balance reference point 23

Figure 2.2 Schematic of the model and wind axes 24

Figure 2.3 Flowchart of the uncertainty analysis 24

Figure 2.4 Structure of the uncertainty analysis algorithm within the data reduction routine 30

Figure 3.1 95-percent uncertainty bands on coefficient of drag 34

Figure 3.2 Upper and lower 95-percent uncertainty curves for coefficient of drag 34

Figure 3.3 Upper and lower 95-percent uncertainty curves for coefficient of lift 35

Figure 3.4 Coefficient of drag 95-percent uncertainty 36

Figure 3.5 Coefficient of lift 95-percent uncertainty 36

Figure 3.6 Coefficient of drag of two different model configurations tested under similar conditions 37

Figure 3.7 Coefficient of drag 95-percent uncertainty comparison between two different model configurations tested under similar wind tunnel operating conditions 38

Figure 3.8 Coefficient of lift of two different model configurations tested under similar conditions 38

Figure 3.9 Coefficient of lift 95-percent uncertainty comparison between two different model configurations tested under similar wind tunnel operating conditions 39

Figure 3.10 Coefficient of drag 95-percent uncertainty at different operating conditions 40

Figure 3.11 Coefficient of lift 95-percent uncertainty at different operating conditions 40

Figure 3.12 Coefficient of drag 95-percent uncertainty at different Mach numbers 41

Figure 3.13 Test section freestream Mach number 95-percent uncertainty 42

Figure 3.14 Test section freestream dynamic pressure 95-percent uncertainty 43

Figure 3.15 Systematic, random and total 95-percent uncertainty of coefficient of drag 44

Figure 3.16 Systematic, random and total 95-percent uncertainty of coefficient of lift....44

Figure 3.17 Breakdown of contributions for coefficient of drag total uncertainty 46

Figure 3.18 Breakdown of contributions for coefficient of lift total uncertainty....46

Figure 3.19 Breakdown of contributions for coefficient of lift total uncertainty of an alternative model configuration at low speed condition....47

Figure 3.20 Breakdown of contributions for coefficient of lift total uncertainty of an alternative model configuration at high speed condition....48

Figure 3.21 Breakdown of contributions for coefficient of drag random uncertainty ..51

Figure 3.22 Breakdown of contributions for coefficient of lift random uncertainty.....51

Figure 3.23 Systematic, random and total 95-percent uncertainty of Mach number 53

Figure 3.24 Systematic, random and total 95-percent uncertainty of dynamic pressure 53

Figure 3.25 Breakdown of contributions for Mach number random uncertainty 54

Figure 3.26 Breakdown of contributions for dynamic pressure random uncertainty....55

Figure 3.27 Monte Carlo simulation process 57

Figure 3.28 Comparison of TSM and MCM estimates of total uncertainties 57

Figure 3.29 Comparison of TSM and MCM estimates of random uncertainties 57

Figure 3.30 Mach number uncertainty validation 60

Figure 3.31 Dynamic pressure uncertainty validation....61

Figure 3.32 Mach number random uncertainty and observed variability as percentage of the nominal Mach 61

Figure 3.33 Dynamic pressure random uncertainty and observed variability as percentage of the nominal dynamic pressure 62

Figure 3.34 Measurements of settling chamber stagnation pressure and test section static pressure during a low speed run 63

Figure 3.35 The trend in random variations of stagnation and static pressures in a low speed run 63

Figure 3.36 Coefficients of drag of a pair of high speed repeat runs 65

Figure 3.37 Random uncertainty and variability in drag coefficients of a pair of high speed repeat runs 65

Figure 3.38 Coefficient of drag random uncertainty validation 67

Figure 3.39 Coefficient of lift random uncertainty validation 67

LIST OF ABBREVIATIONS

AIAA	American Institute of Aeronautics and Astronautics
DRE	Data Reduction Equation
Eq	Equation
MCM	Monte Carlo Method
NRC	National Research Council
TSM	Taylor Series Method
UPC	Uncertainty Percentage Contribution

LIST OF SYMBOLS AND UNITS OF MEASUREMENTS

Symbols

a	model wing span (in)
A_w	model wing area (in^2)
b	bias limit of an independent variable
b'	correlated bias error
B	95-percent confidence systematic uncertainty
c	model wing chord (in)
$C_{d\ nac}$	nacelle drag coefficient
C_D	drag coefficient
C_L	lift coefficient
C_{pm}	pitch coefficient in model axis
C_{pmw}	pitch coefficient in wind axis
C_{rm}	roll coefficient in model axis
C_{rmw}	roll coefficient in wind axis
C_x	axial force coefficient
C_{ym}	yaw coefficient in model axis
C_{ymw}	yaw coefficient in wind axis
C_z	normal force coefficient
$\overline{E}$	mean error of calibration
F	force (lb)
i, m, n	index of an independent variable
J	number of independent variables

k	index of an elemental bias error
L	number of elemental bias error sources
M	calculated test section Mach number
N	number of calibration data points
N_1, N_2, N_3	normal force component of the balance (lb)
P	pressure (psi)
P_0	total or stagnation pressure (psi)
P_A	atmospheric pressure (psi)
P_I	test section static or freestream pressure (psi)
q	calculated dynamic pressure (psi)
r	experimental result parameter
$\overline{R}$	average range of result
Re	Reynolds number
s	precision limit of an independent variable
S	95-percent confidence random uncertainty
S_E	standard deviation of calibration residuals
U, $U_{95\%}$	Total 95-percent confidence uncertainty
U_{ws}	uncertainty of the calibration working standard
x	independent variable
X_1, X_2	axial force component of the balance (lb)
y_{nac}, z_{nac}	nacelle moment arm (in)
y_{ref}, z_{ref}	balance reference to model reference distance (in)
α	angle of attack (degree)

σ	standard deviation of result

Units

ft	foot
in	inch
lb	pound
m	meter
psi	pound per square inch
sec	second

INTRODUCTION

Accurate prediction of aircraft aerodynamic performance is critical to manufacturers like Bombardier Aerospace for design and development activities. Even though advances in computing power, modeling approaches, and computational fluid dynamic algorithms can now provide performance estimates, wind tunnel experimental data are still required for validation of the analytical results. It is critical that the degree of goodness of the collected data or the data uncertainty be considered, as the uncertainty interval effectively sets the resolution at which comparisons can be made between experimentally obtained data and simulation results (Coleman and Steele, 2009).

The contributing factors to the total uncertainty at a wind tunnel are the error sources related to data acquisition, data processing, calibration and math models used to adjust data, as well as the geometry and surface finish of the test article. Spatial flow nonuniformity, flow unsteadiness, wall interference and buoyancy effects are among the aspects of the test environment which further contribute to the overall uncertainties of the result (AIAA, 1999). Developing a methodology for estimating the combined effect of such factors or the measurement uncertainty is the first step in data quality assessment and control at any test facility, as data quality can only be improved once it is properly quantified. Such methodologies have been implemented already at many wind tunnels in North America including those at the NASA Langley, Marshall, Glenn and Ames Research Centers (Walter, Lawrence and Elder, 2010; Springer, 1999; Stephens et al, 2016; Ulbrich and Boone, 2004).

The primary objective of the present master's project is to equip the National Research Council (NRC) 1.5 m trisonic wind tunnel with an error propagation model that would estimate the uncertainty of all the result parameters in the Bombardier half-model experiments, and report them in the form of 95-percent confidence intervals around the measured values, following the methodology recommended by the American Institute of Aeronautics and Astronautics (AIAA) Standard S-071A-1999. The AIAA Standard (1999) on the assessment of experimental uncertainty presents a practical framework for quantifying

and reporting uncertainty in wind tunnel testing. Guidelines are given on how to estimate the random and systematic errors of the measured variables, which propagate through the data reduction equations to yield the uncertainties of the experiment results. However, no particular strategy is offered for the implementation of the recommended error propagation methodology for a specific test facility. The phases of the present thesis project involved understanding the measurement system and the structure of the data reduction routine of the Bombardier half-model experiments, identifying the independent variables of the data reduction equations, estimating the corresponding precision and bias errors, and finally developing an algorithm for propagating the errors through the data reduction equations in order to obtain and report the uncertainties of the test results. The focus has been on automating the uncertainty analysis process by implementing the error propagation methodology within the existing data reduction routine so that the analysis can be performed at every measurement point throughout an experiment, over a range of test conditions, model configurations, and model attitudes. The developed algorithm also provides different breakdowns of the uncertainties, in order to investigate the contribution of the individual variables, and also to separate the effect of systematic errors from that of random errors. Such breakdowns can be used to prioritize data quality improvement initiatives.

It should be emphasized that the analysis is limited to the Bombardier half-model experiments, and only reflects the errors of the data acquisition and reduction processes rather than the overall facility performance. The features and the analytical capabilities of the developed algorithm are demonstrated in this report, using the best available estimates of the bias and precision errors of the measured variables and the data of a number of runs from the series of Bombardier experiments performed in February 2014. Figure 0.1 shows an example of a typical experiment setup where a Bombardier half-model is installed in the transonic test section of the NRC 1.5 meter wind tunnel.

Figure 0.1 A Bombardier half-model installed in the 1.5 by 1.5 m transonic test section of the NRC wind tunnel

Taken from Orchard et al. (2007, p. 31)

CHAPTER 1

BACKGROUND

1.1 Facility Description

The NRC 1.5 m blowdown trisonic wind tunnel has a speed range of Mach 0.1 to 4.25. A schematic of the facility is shown in Appendix I. The compressor plant delivers 45 lb/sec of filtered dry air at 312 psi to three air storage vessels. When a run is initiated, air flows from the storage tanks to the settling chamber. The flow is regulated by a control valve to maintain the settling chamber stagnation pressure within 0.5 percent of the set point value during a run. A large matrix of long steel tubes placed at the outlet of the air storage keeps the temperature of the outflowing air at a nearly constant value to minimize Reynolds number changes. After passing through acoustic baffles and turbulence screens, the air accelerates in a nozzle, whose flexible plates are set to achieve a desired test section Mach number. Downstream of the test section, the air is slowed down through a variable diffuser and discharged through an exhaust silencer to atmosphere (Brown, 1977). In subsonic and transonic operations, the servo-controlled throat area of the downstream variable diffuser establishes the nominal test section Mach within very close limits.

In half-model experiments, the test article is mounted with a reflection plane on the half-model sidewall force balance in the 1.5 by 1.5 m transonic test section with perforated walls. The balance consists of three normal and two axial strain gauged flexure elements, which allow the overall forces and moments to be measured. The balance also provides the means of varying the pitch attitude. A diagram of the half-model balance is presented in Appendix II. Data acquisition of a typical test consists of a number of wind-off data collections or tares, followed by the wind-on run data recording. A wind-off duplicate of the run, with the model pitching, is used to subtract inertial forces or weight contributions from the wind-on data in order to obtain the true aerodynamic loads. Other tare data are used for checking the calibration of the pressure measurement instruments. Table 1.1 summarizes the most common operating conditions of the half-model experiments carried out by Bombardier

in terms of nominal test section Mach number M, Reynolds number Re in million per foot, settling chamber pressure P_0 set point, and the expected test section static and dynamic pressures, P_I and q.

Table 1.1 Common nominal test conditions of Bombardier half-model experiments

M	Re (10^6/ft)	P_0 (psi)	P_I (psi)	q (psi)
0.2	8.4	90.88	88.38	2.47
0.85	6.2	21.27	13.26	6.71
0.9	6.2	20.78	12.29	6.97
0.925	6.2	20.57	11.83	7.09
0.97	6.2	20.25	11.07	7.29

1.2 Uncertainty Analysis Overview

Error is the difference between a measured quantity and its true value, caused by an error source. It is assumed that each error whose sign and magnitude are known have been removed by correction. Any remaining error is therefore of unknown sign and magnitude (Coleman and Steele, 2009). Lower error is associated with higher accuracy, as accuracy indicates the closeness of the experimentally obtained value to the truth (AIAA, 1999). However, since the true value of a quantity is generally unknown, both error and accuracy are qualitative terms. Uncertainty U is a quantified estimate of the error, based on statistical analysis, experience and judgment. An uncertainty interval is a range within which the actual but unknown value of an error is believed to fall, with a certain confidence. The estimates are commonly reported at a 95-percent confidence level (AIAA, 1999), meaning the true value of a quantity is expected to be in the bracket defined by $\pm U$ around the obtained experimental value, 95 times out of 100. Uncertainty analysis is a strategic approach to describing the degree of goodness of a measurement or an experimental result by quantifying the error

associated with the obtained value in the form of a 95-percent confidence uncertainty interval.

Error sources are categorized as systematic and random, also known as bias and precision, respectively. A systematic or bias error is an error that does not vary during the measurement period, while a random or precision error is an error that does vary. As shown schematically in Fig. 1.1, the probability distribution of a sample of successive measurements of a variable will have a large number of measured values near the mean of the sample. The bias error appears as an offset of the sample mean from the true value, while the random errors appear as scatter in the measurements and dictate the width of the distribution. The total error of a single measurement or the difference between the measured value and the true value is the sum of the random error of that particular measurement and the overall bias. The uncertainty interval defined around the measured value is then the estimate of the range within which the total error falls 95 percent of the time.

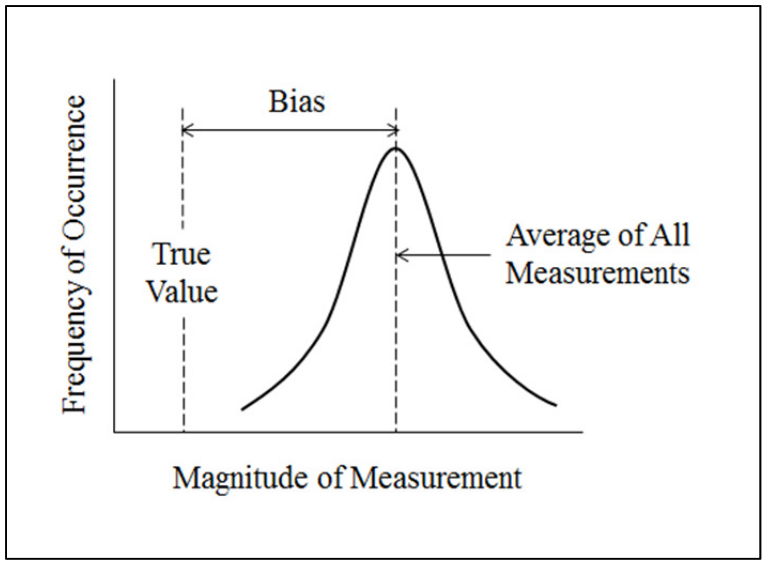

Figure 1.1 Effect of errors in a sample of successive measurements of a variable

Adapted from AIAA Standard (1999)

Contrary to a common misconception, the effects of systematic errors cannot be removed by calibration (Coleman and Steele, 2009). No calibration process is ever perfect, as there are uncertainties associated with the working standard against which an instrument is calibrated. Through calibration, the systematic errors can be reduced, but not eliminated. Bias sources in an experiment are related to residual errors after calibration, data acquisition methods, operator interaction, conceptual errors and math models used to adjust data (Walter, Lawrence and Elder, 2010). On the other hand, the random or precision errors are due to inability to obtain the exact same measurement twice, as a result of the effects such as noise, dynamic behavior of the instrument, or unidentified systematic uncertainties that present as random (Stephens et al., 2016).

To estimate the precision error in measurements of variable x_i, a precision limit s_i is defined. The interval $\pm s_i$ about a measurement of x_i is a band within which the biased mean value of a variable would fall 95 percent of the time (AIAA, 1999). Since precision errors appear as scatter in successive measurements made under nominally identical conditions, the precision limit or the random uncertainty can be best estimated as a standard deviation of repeated measurements multiplied by a coverage factor of 2 for a 95-percent confidence level. The precision limit therefore represents the degree of measurement repeatability. It should be noted that random error sources are generally assumed to be uncorrelated, and to have a Gaussian error distribution (AIAA, 1999; Coleman and Steele, 2009).

Similarly, a bias limit b_i is defined to estimate the bias error in measurements of variable x_i. The estimate is typically based on instrument manufacturer's uncertainty specifications, accuracy of the calibration standards, errors associated with the instrument calibration process and curve fitting procedures, as well as engineering judgment from previous experience (AIAA, 1999). Bias errors from sources that are not independent of each other are assumed to be correlated. For example, two variables that are measured using the same instrument, or using different instruments that have been calibrated against the same standard share a common bias error source. The portions of the bias limits of these two variables that arise from the same source are treated as fully correlated (AIAA, 1999).

Many experimental results are not directly measured but rather determined by an expression involving multiple measured variables and constants, known as the data reduction equation (DRE). Dimensionless groups such as Mach number and force coefficients are examples of result parameters that are obtained from data reduction equations. For a result r given by a DRE of the form

$$r = r(x_1, x_2, ..., x_J) \tag{1.1}$$

the bias and precision limits or the uncertainties in the measured variables x_1, x_2, ..., x_J propagate through the data reduction equation to yield the uncertainty associated with r (taken from Coleman and Steele, 2009). The uncertainties are commonly reported at a 95-percent confidence level in the form of a $\pm U_{95\%}$ uncertainty interval around the measured value, as the range within which the experimenter is 95-percent confident the true value of the result lies (AIAA, 1999; Coleman and Steele, 2009). The two commonly used error propagation approaches to estimating the uncertainty of result parameters are the Taylor Series Method and the Monte Carlo Method (Coleman and Steele, 2009).

In the Taylor Series Method (TSM), the combined 95-percent uncertainty U_r of the result parameter r is given by

$$U_r^2 = \sum_{i=1}^{J} \left[\left(\frac{\partial r}{\partial x_i} s_i \right)^2 + \left(\frac{\partial r}{\partial x_i} b_i \right)^2 \right] + (\text{bias correlation effects}) \tag{1.2}$$

where x_1, x_2, ..., x_J are the independent variables of the data reduction equation of r, while s_i and b_i are respectively the corresponding 95-percent confidence precision and bias limits of variable x_i (adapted from Coleman and Steele, 2009).This expression is a linearized Taylor series expansion about the true result. The partial derivatives represent the sensitivity of the uncertainty of the result to each variable, and are evaluated at the measured values of x_i's. The bias error correlation term corrects the combined uncertainty for the effects of the

correlated bias errors in variables that share a common bias error source. The calculated U_r is an estimate of the standard deviation for the population of possible values of the result r (Coleman and Steele, 2009). More details on TSM propagation will be provided in the following sections of this report.

In the Monte Carlo Method (MCM), a synthetic population of possible values is generated for the result parameter, by calculating the data reduction equation numerous times with randomly perturbed values of the measured variables (Walter, Lawrence and Elder, 2010). First, an appropriate probability distribution is assumed for every precision and bias error of the measured variables, centered at zero with a standard deviation equivalent to the corresponding bias or precision limit of the respective variables. At every iteration, a random number generator selects an error value from each distribution. The specific errors are added to the measured values of the variables, and the result parameter is calculated using the data reduction equation. Correlated bias errors are simulated by adding the same randomly selected error to the correlated variables on each iteration. The process is repeated a number of times to obtain a distribution of possible values for the result parameter. The standard deviation of this generated population is an estimate of the combined uncertainty of the result (Coleman and Steele, 2009). The MCM error propagation technique does not rely on the linearization of the data reduction equation inherent in the TSM calculations (Walter, Lawrence and Elder, 2010). Also MCM is easier to implement in applications where the data reduction equations are complex or solved iteratively, and the partial derivatives needed for the TSM technique are difficult, if not impossible, to obtain.

A wind tunnel experiment involves a large number of measured variables and desired result parameters. The stagnation and the freestream temperature and pressure, the forces on the test article and the angle of attack are among the many measured variables. The experiment results are commonly reported in terms of dimensionless numbers such as the freestream Mach number, and the key aerodynamic force and moment coefficients. Every step of the data flow from sensors to reported results is a source of error and should be considered when performing an uncertainty analysis (AIAA, 1999). The error sources include those related to

test technique, flow quality, model shape and finish, instrumentation system, and math models used in describing the characteristics of the instrumentation and all the corresponding calculations such as curve fittings and interpolations, or equations involving reference dimensions and transfer distances (AIAA, 1999). Calibration methods, data reduction algorithms, zeroing of readings, electrical noise, vibration effects, signal conditioners and amplifiers, tunnel flow angularity, model installation, and model to balance alignment are only a few of the most significant errors that contribute to the uncertainty of the experimental results (AIAA, 1999). It is important that the effects of all the error sources are captured in the bias and precision limits of the independent variables, as the results of any uncertainty analysis are only as good as the estimates of the errors that are propagated through the data reduction equations to yield the final uncertainties (Stephens et al., 2016).

With so many estimations of elemental uncertainties and propagation to so many result parameters, over a range of test conditions, model configurations and model attitudes, it is highly desired to standardize the uncertainty analysis and automate the process. This is accomplished by developing an effective algorithm that makes use of the existing data reduction system of the wind tunnel and implements an appropriate error propagation model, either the TSM or the MCM. The inputs to such an algorithm are the bias and the precision limits of every independent variable involved in the expressions of the result parameters, in addition to the measured values or the collected experimental data, while the outputs are the 95-percent uncertainties in all the calculated results. The $\pm U_{95\%}$ interval about every experimental value of a result indicates the range within which the true value of the parameter is believed to fall 95 times out of 100. The contribution of the individual measured variables to the overall uncertainty of the results can also be investigated separately, in order to determine what errors are likely to dominate at different test conditions. Hence, the uncertainty propagation technique provides an analytical basis for identifying opportunities for data quality improvement. However, it should be acknowledged that the analysis is limited to the data reduction process, and does not reflect the overall facility performance (Walter, Lawrence and Elder, 2010).

1.3 Review of the Literature

At the National Transonic Facility of the NASA Langley Research Center, Walter, Lawrence and Elder (2010) have developed an uncertainty analysis model based on the Monte Carlo technique to estimate the uncertainty of the data reduction process. Their focus has been on data variability or the random component of uncertainty to allow them to compare the developed model with the ongoing statistical data quality control techniques at the National Transonic Facility which are currently used while a test is in progress. For their analysis, the bias limits of the measured variables are estimated from calibrations while numerous benchmark tests were conducted under different operating conditions in order to obtain the precision limits directly based on test data. The variables for which the precision limits were obtained through designated benchmark testing include the balance forces, freestream temperature and pressure, model attitude angle and flow angularity. The precision limits or the random uncertainties in the measurement of these variables showed to increase with dynamic pressure. Walter, Lawrence and Elder (2010) present the calculated random uncertainties of the coefficient of axial force C_A, the coefficient of drag C_D, and the freestream Mach number M and dynamic pressure q, under different test conditions in both air and cryogenic operating modes. The results of the simulations on q and M are compared with the observed variability in the benchmark tests for validation, while those of C_A and C_D are compared with three different measures of variability based on the quality control techniques applied to a large number of tests. Walter et al. (2010) further investigate the contribution of different measured variables to the random uncertainty of C_D and M in order to understand the cause of variability and to define opportunities for improvement. The analysis shows that reducing the random errors in the static pressure and in the normal and axial force measurements would have the largest impact on the variability of these two parameters. Walter et al. emphasize that even though the developed uncertainty model is useful for identifying the most significant error sources, it is limited to the data reduction process and does not reflect the overall facility performance (Walter, Lawrence and Elder, 2010).

At the NASA Marshall Space Flight Center 14 x 14 inch trisonic wind tunnel, Springer (1999) has performed an uncertainty analysis on the tunnel flow parameters and the coefficients of axial and normal force over the entire operation range of the tunnel based on the methodology presented in the AIAA Standard (1999) for the assessment of wind tunnel data uncertainty or the Taylor Series error propagation method. The uncertainty of each of the measured parameters of the data reduction equations is represented by its bias and precision limits. The bias limits are estimated based on the accuracy of the instruments, while the precision limits are obtained from the instrumentation system checks. Springer acknowledges that a detailed uncertainty analysis of the strain gage balance is out of the scope of his work; hence, the bias limits of the force measurements are obtained from the difference between the known check loads applied when the balance is installed in the tunnel and the loads calculated based on the gage voltage readings, while the precision limits are determined from repeat check loads and wind-off runs. The analysis results are reported for the calculated freestream static pressure, Mach number and dynamic pressure over the range of Mach number 0.2 to 2.0. A breakdown of the uncertainty of these flow parameters show that the bias or the systematic component plays the dominant role. As the force coefficients at this wind tunnel are normally computed in the body axis system, Springer focuses on the uncertainty of the coefficients of axial and normal force. Graphs of the total, random and systematic uncertainties for these coefficients indicate a decreasing trend with Mach number and a large contribution by the measurement bias. Springer (1999) claims that in general the uncertainties are within acceptable limits, even though the percentage uncertainties are quite large at low Mach numbers due to the fact that the measured forces are small. A further breakdown of the bias or the systematic uncertainty of the force coefficients reveal that the balance is the major contributor. Hence, Springer (1999) concludes that the strain gage balance requires a full uncertainty analysis.

At the NASA Glenn Research Center 8 x 6 foot supersonic wind tunnel, Stephens et al. (2016) have carried out a Monte Carlo based uncertainty analysis in order to determine the measurement uncertainty of the freestream Mach number. The Monte Carlo Method is chosen due to the complex and highly non-linear nature of the data reduction equations

which involve iterative calculations. The variables that determine Mach number at this tunnel include the calibrated test section static pressure, total pressure in subsonic range, and total pressure downstream of a normal shock in supersonic range. During a test, these pressures are calculated based on a number of pressure measurements at different locations throughout the facility such as the balance chamber, using the predetermined calibration regression coefficients. Hence, the calibration uncertainty of each of these parameters contributes to the overall uncertainty of Mach number, and is determined by considering the uncertainties at the instrumentation level, the random uncertainty of all the measurements, as well as the systematic uncertainty due to spatial non-uniformity. The instrumentation level systematic uncertainty or the bias limit of all the pressure measurements are obtained using an existing Excel based tool which is capable of breaking down the bias error of the instrumentation system into contributions of the separate modules such as the sensor, the signal conditioner, the analog to digital convertor, and the data processor. The random uncertainty or the precision limit of the measurements is obtained from Mach sweep calibration data. Since only a limited number of repeat data points are available, an estimator of standard deviation based on the maximum range of a small sample of measurements is used to represent variability, similar to statistical quality control techniques. Once these elemental uncertainties are determined for each variable, a Monte Carlo simulation is performed to obtain a distribution of possible values around every calculated value of Mach number, whose standard deviation is an estimate of the overall uncertainty. The contribution of different error sources are also studied in the form of several uncertainty breakdowns. Such analyses reveal that the total uncertainty of Mach is largely driven by the systematic component, to which the calibration errors have the largest contribution. Based on the obtained percentage contributions, Stephens et al. provide recommendations for possible improvements. They fully acknowledge however that the uncertainty results are only as good as the estimates of the elemental uncertainties that are propagated (Stephens et al., 2016). They express that additional repeat data or specially designed tests are required in order to obtain more accurate estimates of the precision limits.

At the NASA Ames Research Center 11-foot transonic wind tunnel, Ulbrich and Boone (2004) have developed an algorithm to estimate the uncertainty of the test results based on the Meyn's uncertainty propagation methodology (Meyn, 2000), which is mathematically identical to the TSM technique or that recommended in the AIAA Standard (1999), yet is easier to implement due to its vector formulation. Similar to the TSM approach, the independent variables of the result parameters are identified, and their associated bias and precision errors are obtained from manufacturer specifications, calibrations, and past test experience. Notably, the error of those variables for which no estimates are available is assumed negligible and set to zero. The focus of the analysis is on the uncertainties of Mach number, dynamic pressure and Reynolds number. For the pressure and temperature measurements involved in the expressions of these parameters, the bias limits are estimated using calibration data statistics while the precision limits are extracted from test data. The partial derivatives of the result parameters needed for the error propagation are computed with respect to the independent variables using numerical differentiation with an optimized step size. The precision limits and the partial derivatives are combined to obtain the components of the precision uncertainty vector for each result, while the systematic uncertainty vector is obtained using the bias estimates along with the partial derivatives. The square root of the sum of the norm of the two vectors yields the total uncertainty of the result parameter (Ulbrich and Boone, 2004). An uncertainty percentage contribution is also calculated in the algorithm for every error source, as an indicator of its influence on the overall uncertainty. The calculated uncertainties are reported for Mach number, dynamic pressure and Reynolds number, each as a function of the respective parameter, at different total pressure set points. To conclude, Ulbrich and Boone (2004) emphasize on the importance of obtaining accurate estimates of the elemental uncertainties or the bias and precision limits of the measured variables, expressing that the analysis can be improved once better estimates become available.

At the Naval Surface Warfare Center hypervelocity wind tunnel, Kammeyer (1999) implements the measurement uncertainty analysis technique of the AIAA Standard (1999) or the Taylor series method in the existing data reduction routine. He emphasizes on the efforts

made to automate the process and on the implementation strategy rather than generalizing the state of data quality at the wind tunnel. The bias limits of the measured variables are obtained from calibration data by considering the uncertainty of the working standards against which the instruments are calibrated and also the standard error of the least-square fit to the calibration data, or the calibration residuals. The precision limits on the other hand are estimated from tare data recorded prior to each run. For example, the bias of the force balance is derived from the calibration residuals or the difference between the calculated loads and the loads applied by weight sets of calibration, while the precision is estimated statistically from 10 repeat tares as the largest standard deviation in the pitch angle range. This method is believed to account for the contributions of the model/balance installation, the cabling, and the signal condition to the error of the balance measurements (Kammeyer, 1999). No uncertainty is associated with the reference lengths and areas, or the three-dimensional offset of the model and balance reference centers involved in the data reduction equations. A Taylor series expansion is used to propagate the input errors to the final uncertainty of the results, with the inclusion of terms to account for correlated bias errors. The bias of the common working standard is taken as the correlated value for any measurement instruments that were calibrated simultaneously. The partial derivatives involved in the expressions are computed using finite differences, as the data reduction equations include real gas thermodynamics and are solved iteratively. The calculations are performed over the complete angle of attack range, and the contribution of individual variables to the total uncertainties are reported along with the results. The analysis reveal that the uncertainties vary significantly over the pitch sweep as they depend on the force and the angle of attack measurements. Kammeyer (1999) acknowledges that the focus of his work was not on the uncertainty of the force balance, but rather on implementing an automated process for determining the overall uncertainty of the results based on the best available estimates of the bias and precision errors of the measured variables. However, the balance appears as the dominant contributor to the uncertainties and Kammeyer (1999) recommends that any attempts to improve data quality should focus on the balance calibration to reduce the bias.

1.4 Objectives

The objective of the present project is to implement the methodology recommended by the AIAA Standard (1999) on the assessment of experimental uncertainty at the NRC 1.5 m trisonic wind tunnel in order to determine the uncertainty of all the result parameters in the Bombardier half-model experiments in the form of 95-percent confidence intervals around the measured values. The approach involves estimating the bias and precision errors of the key measured variables, and developing an algorithm to propagate these errors through the data reduction routine to obtain the uncertainties associated with the experiment results. Moreover, it is desired to identify the variables that have the largest contribution to the overall uncertainties and deserve the most attention in any future data quality improvement initiatives.

CHAPTER 2

METHODOLOGY

2.1 Analysis Fundamentals

The effects of elemental error sources inherent in the measurement system are captured in bias and precision limits defined around every single reading of the individual components. Following the methodology presented in the AIAA Standard (1999), bias and precision limits for the measured values of independent variables such as force, pressure and angle of attack are estimated based on the latest tunnel calibration data and the uncertainty of the working standards used in the calibration process. Once those are obtained, the Taylor Series Method is used for propagation of the uncertainties of measured variables through the data reduction equations in order to calculate the overall uncertainty associated with each of the experiment parameters such as Mach number, dynamic pressure and the resultant force and moment coefficients.

For an experimental result r given by a data reduction equation of the form

$$r = r(x_1, x_2, ..., x_J) \tag{2.1}$$

where x_1, x_2, ..., x_J are the independent variables, the total 95-percent confidence uncertainty in the result is defined by the root-sum-square of the total random and systematic uncertainties, S_r and B_r as follows

$$U_r = \sqrt{S_r^2 + B_r^2} \tag{2.2}$$

(taken from AIAA Standard, 1999). The 95-percent confidence random uncertainty of the result is calculated as,

$$S_r^2 = \sum_{i=1}^{J} \left(\frac{\partial r}{\partial x_i} s_i \right)^2 \tag{2.3}$$

where s_i is the precision limit of the independent variable x_i. The correlated random errors are conventionally neglected in this equation (AIAA, 1999; Coleman and Steele, 2009). Assuming a large sample size and a Gaussian error distribution,

$$s_i = 2S_{E,i} \tag{2.4}$$

where $S_{E,i}$ is the standard deviation of the calibration residuals for measured variable x_i (AIAA, 1999). Similarly, the 95-percent confidence systematic uncertainty of the result is obtained by propagation of bias limits as follows (AIAA, 1999)

$$B_r^2 = \sum_{i=1}^{J} \left(\frac{\partial r}{\partial x_i} b_i \right)^2 + 2 \frac{\partial r}{\partial x_m} \frac{\partial r}{\partial x_n} b'(x_m, x_n) \tag{2.5}$$

where $b'(x_m, x_n)$ is the covariance term for each (x_m, x_n) pair of independent variables whose bias errors are believed to be correlated, and is approximated by

$$b'(x_m, x_n) = \sum_{k=1}^{L} (b_m)_k (b_n)_k \tag{2.6}$$

where L is the number of elemental systematic error sources, b_m and b_n, that are common in measurements of x_m and x_n. Following the AIAA Standard (1999), the bias limit of the measured variables is estimated from the latest calibration data as the uncertainty of the measurement system during calibration

$$b_i = \left[U_{ws}^2 + \bar{E}^2 + \left(\frac{2S_{E,i}}{\sqrt{N}} \right)^2 \right]^{1/2} \tag{2.7}$$

where U_{ws} is the 95-percent uncertainty of the working standard, $\bar{E}$ is the mean error of calibration, and $S_{E,i}$ is the standard deviation of the individual errors for N readings of variable x_i.

The first step in implementing the described uncertainty analysis methodology is identifying all the independent variables involved in the equations of the result parameters, and estimating their bias and precision limits. The data reduction routine in Bombardier half-model experiments is reviewed in the following section, highlighting the calculations involved in obtaining the result parameters of interest.

2.2 Data Reduction

Data reduction refers to the process of reducing the raw digital data or the readings of all the measurement devices obtained by the data acquisition system to the result parameters of the experiment such as the tunnel operating condition parameters, model state, and the corresponding aerodynamics force and moment coefficients. Once a run is completed, data reduction routine is performed in MATLAB and within a few seconds the output results are tabulated and saved for the client. In Bombardier half-model experiments, the data acquisition system records raw measurements of the settling chamber total or stagnation temperature thermometer, the stagnation pressure P_0, test section freestream static pressure P_I, and atmospheric pressure P_A absolute pressure transducers, the balance accelerometer, the model accelerometer, and the five strain-gaged flexures of the balance, among many other instruments whose measured variables are not directly relevant to the uncertainty analysis work. (For example, there are six pressure measurement rails in the test section, whose readings are used to correct the data for wall interference effects. However, since the uncertainty analysis is only focused on the experiment results prior to the application of the

wall corrections, those variables and their corresponding reduction calculations are not included in the discussions.) At the initial stages of the data reduction routine, calibration factors and offset are applied to convert the measurements, commonly recorded in volts, to engineering units such as psi, degree and lb. The continuous motion run data is next broken down into discrete steps at half-degree pitch angle increments, and the following computations are performed at every step, yielding what will be referred to as a data point.

The tunnel parameters of interest representing the operating condition include the test section Mach number M and dynamic pressure q which are calculated using the isentropic flow relations as shown in Eq. (2.8) and Eq. (2.9)

$$M = \left[5\left(\left(\frac{P_0}{P_1} \right)^{2/7} - 1 \right) \right]^{1/2} \tag{2.8}$$

$$q = 0.7 \frac{P_0 M^2}{\left(1 + 0.2M^2\right)^{7/2}} \tag{2.9}$$

Before substitution, the measured stagnation pressure P_0 and freestream pressure P_1 are tared against the atmospheric pressure P_A for improved accuracy. Test section Reynolds number is another parameter that defines the nominal test condition but it is not investigated in the present uncertainty analysis. Hence, stagnation temperature which appears only in the equation of Reynolds number (through air density and viscosity) is also irrelevant to this analysis.

The model attitude or the angle of attack α at every step is calculated from the balance accelerometer measurement using the previously determined calibration factors. The readings of the secondary accelerometer installed inside the model, or the model accelerometer, are only used if the balance accelerometer fails during a run. The calculated angle of attack is corrected for flow angularity. The correction value is obtained through tunnel calibration as a function of the control valve position for a given nominal operating condition.

The balance five strain gage bridge readings are converted to force measurements in data reduction by applying the balance calibration matrix. The readings are also corrected for interactions between the strain gages through this process. Figure 2.1 shows the location of the strain gage flexures relative to the balance reference point, and their corresponding force components. N_1, N_2 and N_3 are normal force, and X_1 and X_2 are axial force components in the model axis coordinate system. Next, the model weight contributions are subtracted from the measurements to obtain the net aerodynamic loads at each step.

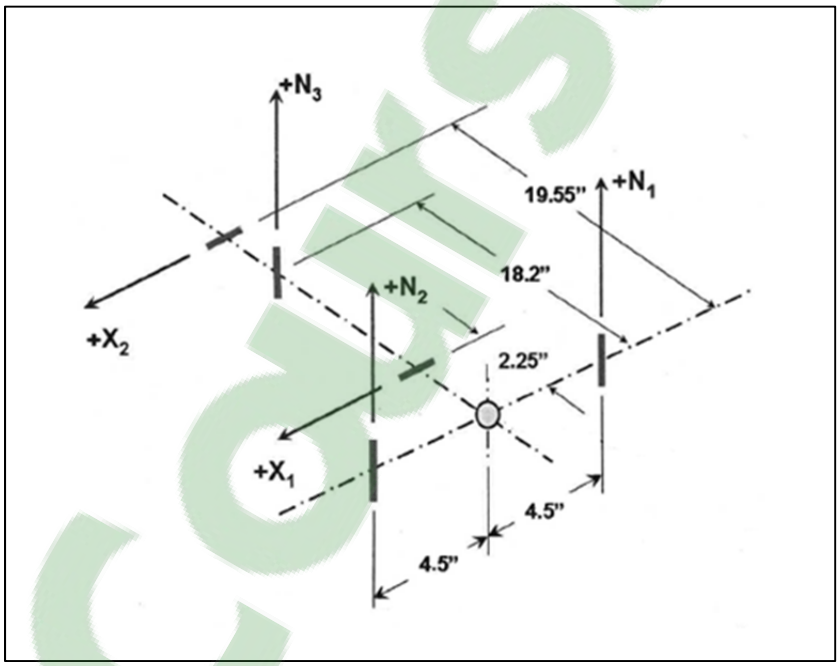

Figure 2.1 Location of the balance force components relative to the balance reference point

Taken from Orchard et al. (2007, p. 36)

The final results of every run are reported in terms of non-dimensional aerodynamic force and moment coefficients in both model and wind axis coordinate systems. As seen in Figure 2.2, the wind axis is defined parallel to the tunnel air flow and is fixed, while the model axis moves with the test article and the balance as the model attitude or the angle of attack α is varied throughout a run.

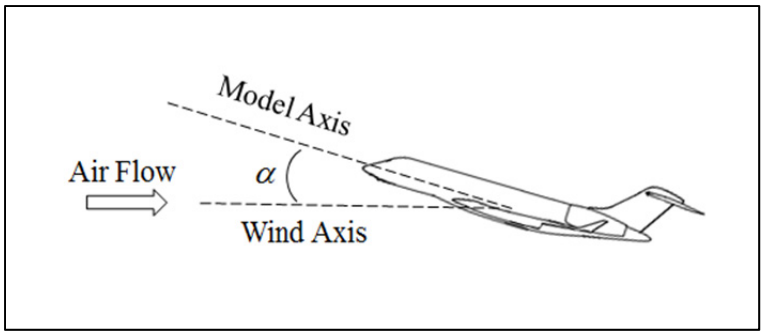

Figure 2.2 Schematic of the model and wind axes

In the model axis coordinate system, also known as the body axes, the result parameters are the coefficients of normal and axial force, C_z, and C_x, and the non-dimensional pitch, yaw and roll moments, C_{pm}, C_{ym}, and C_{rm}. The simplified data reduction equations for these parameters are presented in Eq. (2.10) to Eq. (2.14) which are carried out at every step to form data points.

$$C_z = \frac{N_1 + N_2 + N_3}{qA_w} \tag{2.10}$$

$$C_x = \frac{X_1 + X_2}{qA_w} - C_{d_{nac}} \tag{2.11}$$

$$C_{pm} = \frac{4.5(N_1 - N_2) + z_{ref}(X_1 + X_2)}{qA_w c} - \frac{z_{nac} + z_{ref}}{c} C_{d_{nac}} \tag{2.12}$$

$$C_{ym} = \frac{-(2.25 + y_{ref})X_1 - (19.55 + y_{ref})X_2}{2qA_w a} + \frac{y_{ref} - y_{nac}}{2a} C_{d_{nac}} \tag{2.13}$$

$$C_{rm} = \frac{18.3N_3 + y_{ref}(N_1 + N_2 + N_3)}{2qA_w a} \tag{2.14}$$

At each step, N_1, N_2, N_3, X_1 and X_2 are the fully corrected measurements of the five force components of the balance, and q is the dynamic pressure calculated based on the tare corrected P_0 and P_1. $C_{d\,nac}$ is the nacelle drag coefficient which is provided by Bombardier as a function of Reynolds and Mach number, and is available as a look-up table to the data

reduction routine. The drag value is treated as a constant and is subtracted from the axial force readings. The reference dimensions z_{nac}, and y_{nac} are the transfer distances or the moment arms for the nacelle drag force to a reference point on the model, while z_{ref}, and y_{ref} are the distances from the balance reference point to the model reference point, all in inches. The model dimensions A_w, c, and a are wing area, mean aerodynamic chord, and span respectively.

In the wind axis coordinate system, the result parameters are the coefficient of lift C_L, the coefficient of drag C_D, and the non-dimensional pitch, yaw and roll moments, C_{pmw}, C_{ymw}, and C_{rmw}. The simplified data reduction equations for these parameters are provided by Eq. (2.15) to Eq. (2.19).

$$C_L = C_z \cos\alpha - C_x \sin\alpha \tag{2.15}$$

$$C_D = C_z \sin\alpha + C_x \cos\alpha \tag{2.16}$$

$$C_{pmw} = C_{pm} \tag{2.17}$$

$$C_{ymw} = C_{ym} \cos\alpha - C_{rm} \sin\alpha \tag{2.18}$$

$$C_{rmw} = C_{ym} \sin\alpha + C_{rm} \cos\alpha \tag{2.19}$$

The angle of attack α is the model attitude at every step, corrected for flow angularity.

2.3 Elemental Errors

The result parameters defined by Eq. (2.8) through (2.19) are the focus of the present uncertainty analysis. The primary independent variables of these data reduction equations include the settling chamber total or stagnation pressure P_0, the test section freestream pressure P_I, the model pitch angle or the angle of attack α, and the balance normal N_1, N_2, N_3, and axial X_1, X_2 force components. Table 2.1 summarizes the bias and precision limits of these variables which are obtained from the calibration of the respective measurement devices and the checks performed at the beginning of the experiment.

Table 2.1 Estimates of the bias and precision limits of the independent variables

Variable	Bias Limit	Precision Limit
P_0 (psi)	0.0071	0.0136
P_1 (psi)	0.0068	0.0075
α (degree)	0.017	0.010
N_1 (lb)	1.038	0.399
N_2 (lb)	1.080	0.627
N_3 (lb)	1.024	0.480
X_1 (lb)	1.003	0.660
X_2 (lb)	1.004	0.460

The contributors to the bias error are considered to be the uncertainty of the working standard against which the instrument is calibrated as well as the mean and the standard deviation of the calibration residuals. Ideally, the precision limit or the random error would be obtained from repeated measurements of each of the abovementioned independent variables similar to the work of Walter, Lawrence and Elder at the National Transonic Facility (2010); however, in the absence of such a database for the measurement system, the precisions limits have been derived from the standard deviation of the residuals of the main calibrations or the calibration checks carried out prior to the experiment. Since the data acquisition system performs identically under calibration and testing processes, the precision limits obtained from calibration data are believed be a good representation of the effects of the random errors encountered during testing (AIAA, 1999).

The half-model balance was last calibrated in February 2011, and a calibration check was conducted using deadweights in February 2014, before the most recent Bombardier experiment. The uncertainties of each of the five force components are estimated based on the corresponding calibration residuals, or the difference between the loads applied during calibration and the loads calculated from the recorded gage voltages using the calibration matrix (AIAA, 1999). First, the calibration uncertainty of each component is determined by

Eq. (2.7). The uncertainty of the working standard U_{ws} in this equation is set to the specified 1.00 lb uncertainty of the calibration load cell, while $\overline{E}$ and S_E are the average and the standard deviation of the calibration residuals of the respective component. The mean error of the 2014 calibration check is then combined with this calibration uncertainty as root-sum-square to obtain the bias limit of each force component. The precision limit is estimated by Eq. (2.4) from the residuals of the 2014 calibration check, where the balance is installed in the tunnel and the production test routine is used to record and reduce the balance force measurements. Therefore, the error or the observed precision is believed to be an accurate estimate of the balance repeatability during the test to follow. The results are those presented in Table 2.1. Since all the components of the balance are calibrated simultaneously against the same standard, their bias errors are assumed to be fully correlated (AIAA, 1999; Coleman and Steele, 2009). Hence, a covariance term is included for each pair of the balance components in Eq. (2.5) when calculating the systematic uncertainty of the force and moment coefficients, and the uncertainty of the calibration load cell is taken as the common bias.

The pressure transducers are calibrated in two steps, through a process known as transfer calibration. The Paroscientific Digiquartz absolute pressure transducers used for measuring the stagnation pressure P_0 and the test section freestream pressure P_1 are calibrated against another Digiquartz transducer referred to as D5, which is itself calibrated against a Ruska deadweight gauge. The specified uncertainty of the deadweight gauge is ±0.0015% of reading. A single conservative estimate of its uncertainty throughout the calibration process is taken as 0.0015% of the maximum applied pressure which yields ±0.0026 psi. Using the residuals of the first step of the calibration, D5 against the Ruska deadweight gauge working standard, the calibration uncertainty of D5 is calculated through Eq. (2.7) to be ±0.0044 psi. This value is then used as the uncertainty of the working standard U_{ws} at the second step of the calibration, where the readings of P_0 and P_1 transducers are compared against D5. The standard deviation and the mean of the residuals at the second step are used in Eq. (2.7) along with the calibration uncertainty of D5 as U_{ws} to find the bias limits of the measurements of P_0 and P_1. The corresponding precision limits are derived directly from the residuals of calibration against D5 through Eq. (2.4). The numbers presented in Table 2.1 are obtained

from the transfer calibration conducted in January 2014. Since the two transducers are calibrated simultaneously against a common standard, their bias errors are assumed to be fully correlated (AIAA, 1999; Coleman and Steele, 2009). Hence, a covariance term is included in Eq. (2.5) for the two pressure measurements when calculating the systematic uncertainty of the result parameters and the uncertainty of the working standard D5 is taken as the common bias.

The primary accelerometer used to determine the model incidence or the angle of attack, located within the balance shell, was last calibrated in January 2014 against a Wyler bubble inclinometer with a specified uncertainty of ±1 minute of arc, or equivalently ±0.016 degree. Eq. (2.4) and Eq. (2.7) are used to estimate the precision and bias limit of the angle of attack measurements based on the calibration residuals, as reported in Table 2.1.

The other independent parameters in the data reduction equations include the reference dimensions such as the model wing area, chord and span, the axis transfer distances y_{ref} and z_{ref}, in addition to the moment arms of nacelle drag y_{nac} and z_{nac}. As recommended by the AIAA Standard (1999), the bias and precision limits are assumed to be zero for every parameter that is assigned a value. Hence, no uncertainty is introduced into the result by these constants of the data reduction equations. It should be noted that the nacelle drag coefficient is also treated as a constant in the uncertainty analysis as its value is defined by the client. It was confirmed that even assuming a 10% bias error for the value had an insignificant contribution to the overall uncertainty of the experiment results. The effect of the error in the flow angularity correction applied to the angle of attack measurements and in the tare correction applied to the stagnation and freestream pressure readings was also assumed negligible, as the corrected values are used in all the uncertainty computations.

2.4 Implementation

The uncertainty analysis equations have been implemented in MATLAB in the form of additional subroutines that execute within the main data reduction code for the Bombardier

half-model experiments, at every data point and for every result parameter. Figure 2.3 shows a flowchart of the calculations. The estimated uncertainty of the working standards and the bias and precision limits of the independent variables are provided as inputs to the uncertainty algorithm. The partial derivatives of the data reduction equations, or absolute sensitivity coefficients, are derived analytically with respect to the independent variables using the MATLAB symbolic math toolbox. Numerical values of the derivatives are then obtained for the expressions at each data point by substituting the measurements of the independent variables. These derivatives and the limits are combined in the form of Eq. (2.3) and (2.5) to compute the overall uncertainties.

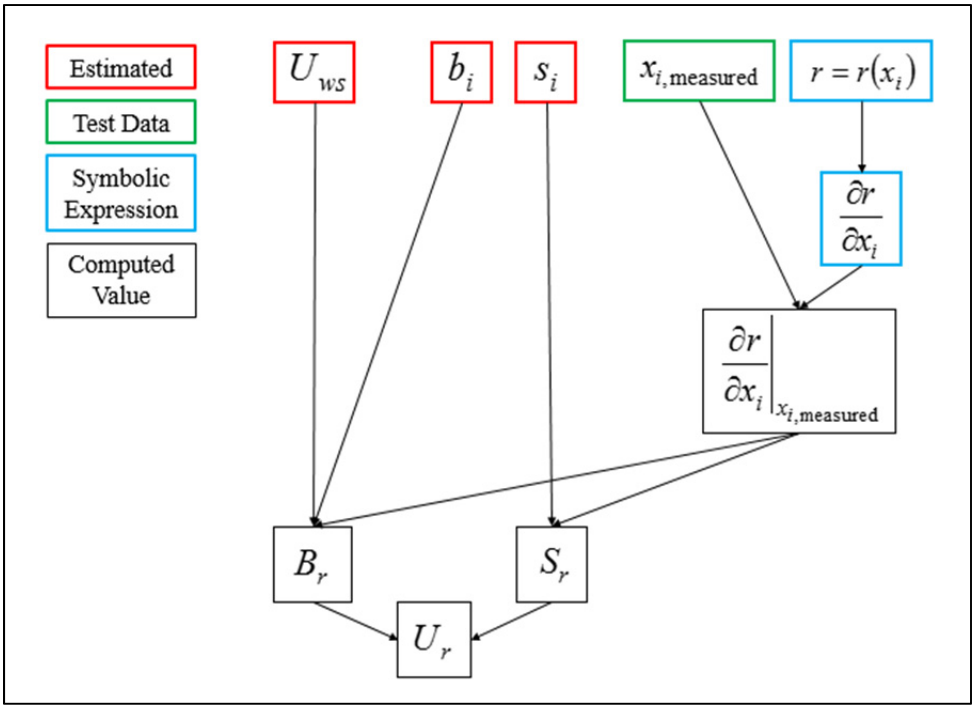

Figure 2.3 Flowchart of the uncertainty analysis

The final outputs of the uncertainty analysis algorithm are the 95-percent systematic, random and total uncertainties in the tunnel parameters and all the force and moment coefficients, which are reported along with the test data. In further stages, the uncertainty percentage contributions of the primary independent variable are also obtained to indicate their influence on the uncertainty of the results. A diagram of the algorithm structure is provided in

Figure 2.4 to introduce the developed MATLAB functions which accomplish the steps of the flowchart. The high level functions of the existing data reduction routine are shown in gray merely to illustrate and emphasize the implementation process.

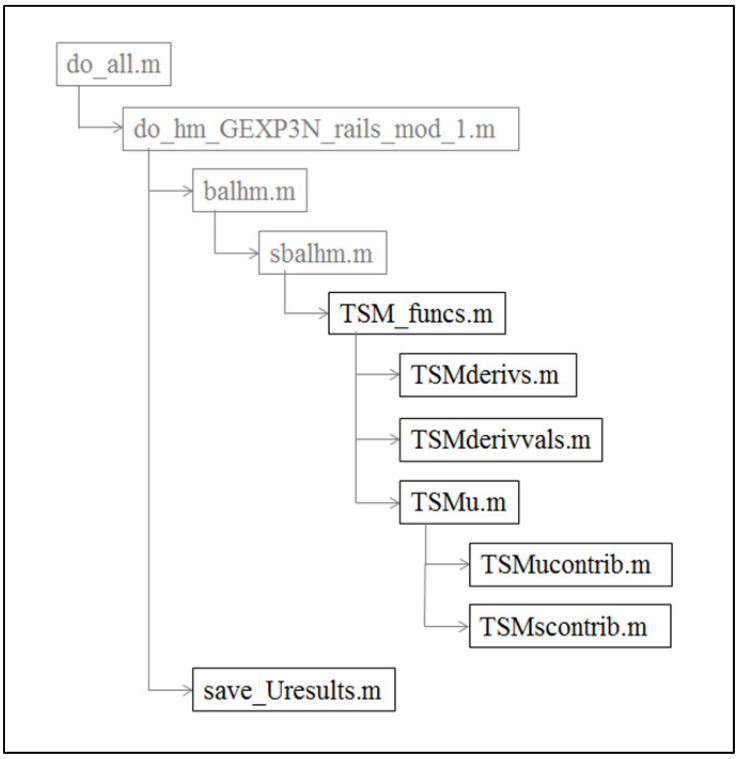

Figure 2.4 Structure of the uncertainty analysis algorithm within the data reduction routine

TSM_funcs is the main function of the uncertainty analysis where the bias and precision limits of all the independent variables and the working standard uncertainties are defined. The measurements of the independent variables at a given step and the constants of the data reduction equations are also provided here as inputs. Once these values are assigned to local variables, other sub-functions are called to perform the uncertainty calculations for all the result parameters. At the first sub-function *TSMderiv*, the data reduction equations are expressed symbolically, similar to Eq. (2.8) to Eq. (2.19). Then the partial derivatives of every result parameter are computed with respect to the relevant independent variables using the symbolic math toolbox. For example, substituting Eq. (2.8) into Eq. (2.9) and Eq. (2.9)

into Eq. (2.10), it can be seen that the independent variables involved in the expression of C_z are P_0, P_I, N_1, N_2 and N_3. Hence, the partial derivatives computed by *TSMderivs* for the uncertainty of C_z include $\partial C_z/\partial P_0$, $\partial C_z/\partial P_I$, $\partial C_z/\partial N_1$, $\partial C_z/\partial N_2$ and $\partial C_z/\partial N_3$ which are obtained through the MATLAB built-in symbolic differentiation function *diff* as *diff(C_z,P_0)*, *diff(C_z,P_I)*, *diff(C_z,N_1)* and so on. At the next sub-function *TSMderivvals*, the numerical values of the partial derivatives are computed using the measurements of the given step and the constants of the equations. In *TSMu*, these numerical values of the partial derivatives and the bias and precision limits of the independent variables are combined in the form of Eq. (2.3) and Eq. (2.5) to compute the 95-percent random and systematic uncertainties of every result parameter, at a given step. The 95-percent total uncertainties are then calculated using Eq. (2.2). For the example of C_z, the expressions would be as follows

$$S_{C_z}^2 = \left(\frac{\partial C_z}{\partial P_0} s_{P_0}\right)^2 + \left(\frac{\partial C_z}{\partial P_I} s_{P_I}\right)^2 + \left(\frac{\partial C_z}{\partial N_1} s_{N_1}\right)^2 + \left(\frac{\partial C_z}{\partial N_2} s_{N_2}\right)^2 + \left(\frac{\partial C_z}{\partial N_3} s_{N_3}\right)^2 \tag{2.20}$$

$$B_{C_z}^2 = \left(\frac{\partial C_z}{\partial P_0} b_{P_0}\right)^2 + \left(\frac{\partial C_z}{\partial P_I} b_{P_I}\right)^2 + 2\frac{\partial C_z}{\partial P_0}\frac{\partial C_z}{\partial P_I} b'(P_0, P_I) \tag{2.21}$$
$$+ \left(\frac{\partial C_z}{\partial N_1} b_{N_1}\right)^2 + \left(\frac{\partial C_z}{\partial N_2} b_{N_2}\right)^2 + \left(\frac{\partial C_z}{\partial N_3} b_{N_3}\right)^2$$
$$+ 2\frac{\partial C_z}{\partial N_1}\frac{\partial C_z}{\partial N_2} b'(N_1, N_2) + 2\frac{\partial C_z}{\partial N_1}\frac{\partial C_z}{\partial N_3} b'(N_1, N_3) + 2\frac{\partial C_z}{\partial N_2}\frac{\partial C_z}{\partial N_3} b'(N_2, N_3)$$

$$U_{C_z} = \sqrt{S_{C_z}^2 + B_{C_z}^2} \tag{2.22}$$

As seen in Eq. (2.21), a covariance term is included in the expression of systematic uncertainty of C_z for the two pressure measurements in order to account for their correlated bias error since the two transducers were calibrated against a common standard. Similarly, a covariance term exists for every pair of the balance force components (N_1, N_2), (N_1, N_3), and (N_2, N_3) to reflect the effects of simultaneous calibration.

Within the *TSMu* sub-function, *TSMucontrib*, and *TSMscontrib* are called to calculate the percentage contribution of the primary independent variables to the 95-percent total and random uncertainties of the result parameters, respectively. For example, the percentage contribution of pressure to the total uncertainty of C_z is calculated by *TSMucontrib* as

$$\frac{\left(\frac{\partial C_z}{\partial P_0}s_{P_0}\right)^2+\left(\frac{\partial C_z}{\partial P_I}s_{P_I}\right)^2+\left(\frac{\partial C_z}{\partial P_0}b_{P_0}\right)^2+\left(\frac{\partial C_z}{\partial P_I}b_{P_I}\right)^2+2\frac{\partial C_z}{\partial P_0}\frac{\partial C_z}{\partial P_I}b'(P_0,P_I)}{U_{C_z}^2}\times 100 \tag{2.23}$$

while in *TSMscontrib*, the percentage contributions of stagnation pressure and freestream pressure to the random uncertainty of C_z are calculated respectively as

$$\frac{\left(\frac{\partial C_z}{\partial P_0}s_{P_0}\right)^2}{S_{C_z}^2}\times 100 \text{ and } \frac{\left(\frac{\partial C_z}{\partial P_I}s_{P_I}\right)^2}{S_{C_z}^2}\times 100 \tag{2.24}$$

At the end, once the abovementioned functions are executed for every data point, *save_Uresults* tabulates the uncertainty analysis results for all the parameters in an excel file and saves it in the client directory along with the test data.

CHAPTER 3

RESULTS

3.1 Overall Uncertainty Estimates

The data obtained during the most recent series of Bombardier wind tunnel experiments carried out in February 2014 have been used to evaluate the developed uncertainty algorithm. The test was performed using a half-model of a Global business aircraft mounted on the test section side wall in order to investigate the high-lift characteristics and performance of the design. The majority of the runs were performed at Mach 0.2 and unit Reynolds number of 8.4 million per foot, with a few runs at higher speeds, namely Mach 0.85 to 0.97 and Reynolds 6.2 million per foot. It should be noted that the data for angle of attack, freestream Mach number and drag have not been corrected for wall interference effects. The figures presented in this chapter illustrate the result of the uncertainty analysis on the tunnel operating condition parameters, the coefficients of drag C_D and the coefficient of lift C_L measured during selected runs as examples. Actual coefficient values had to be omitted in order to maintain data confidentiality.

The uncertainties in the test results are precisely quantified at every data point over the entire angle of attack range throughout a run as part of the data reduction routine. Figure 3.1 shows the calculated 95-percent confidence interval on the reported coefficient of drag for a portion of a typical C_D curve as error bars on every measurement. Another representation of the uncertainty analysis results can be seen in Figure 3.2 and Figure 3.3, as curves of upper and lower limits on the coefficient of drag and the coefficient of lift.

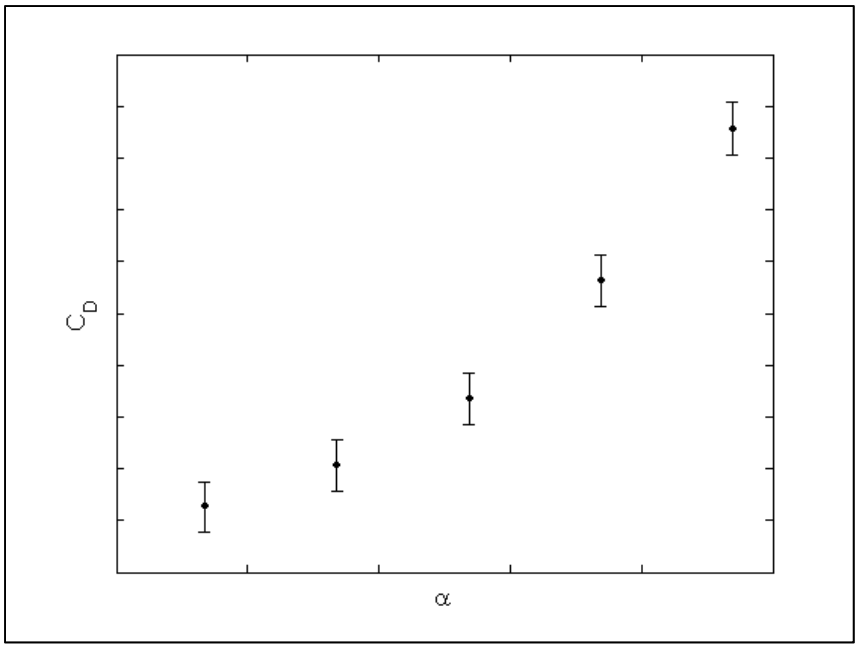

Figure 3.1 95-percent uncertainty bands on coefficient of drag
(α scale = 0.5 degree, C_D scale = 0.002)

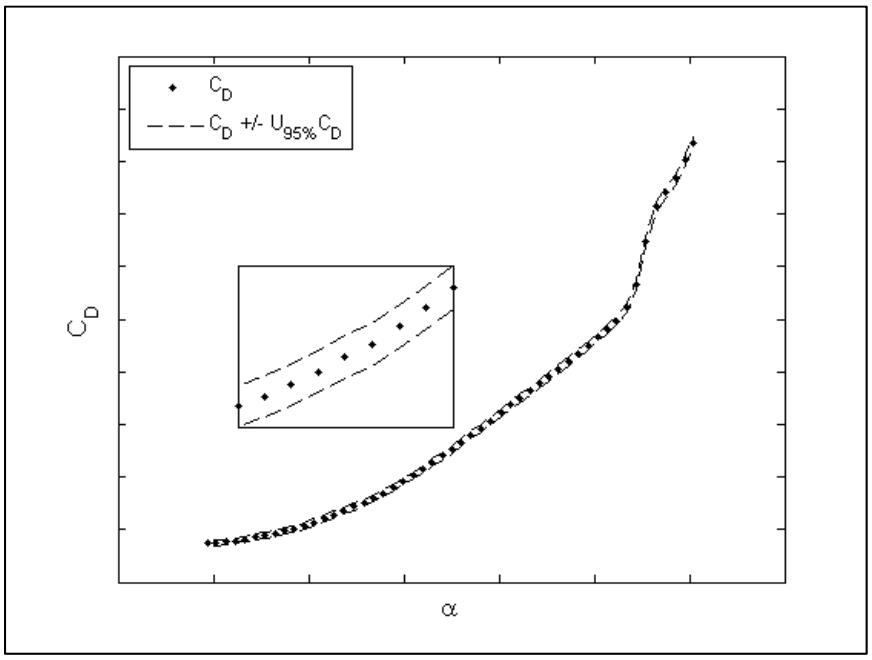

Figure 3.2 Upper and lower 95-percent uncertainty curves for coefficient of drag
(α scale = 5 degrees, C_D scale = 0.05)

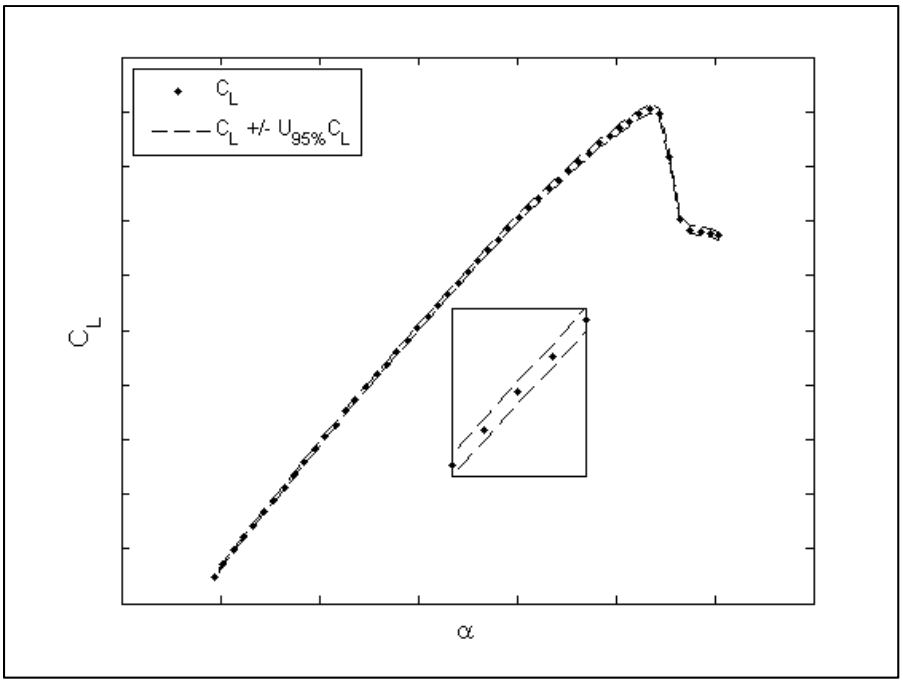

Figure 3.3 Upper and lower 95-percent uncertainty curves for coefficient of lift

(α scale = 5 degrees, C_L scale = 0.2)

The uncertainties in the force and moment coefficients vary over the pitch sweep due to functional dependence on the measured forces and the angle of attack. During the run depicted in Figure 3.2 and Figure 3.3, as C_D and C_L increase with α, the absolute value of total uncertainty increases while the percentage uncertainty decreases. The trend is demonstrated by Figure 3.4 and Figure 3.5 for the overall uncertainty of the coefficient of drag and lift, respectively. The increase in absolute uncertainties is associated with higher measured forces at higher angles of attack.

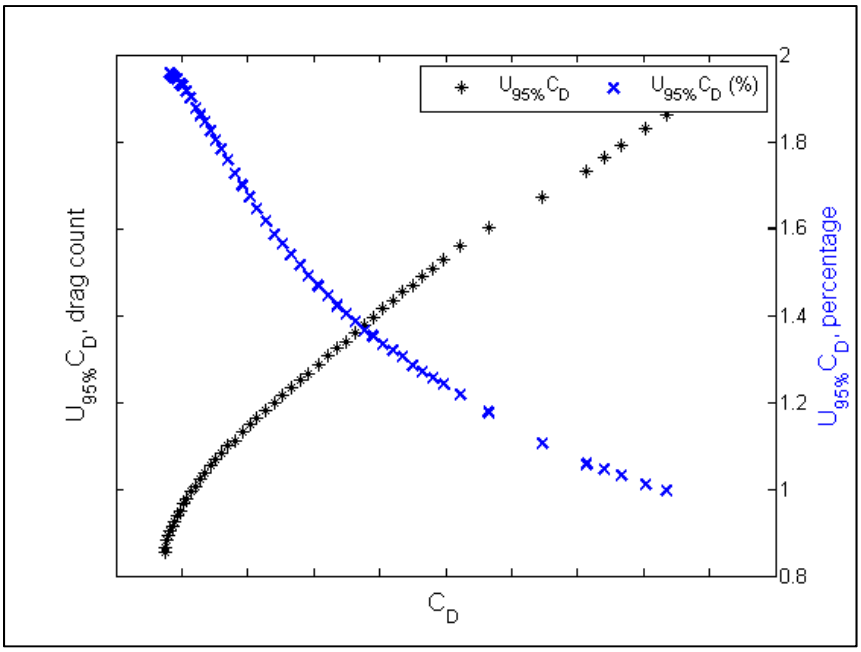

Figure 3.4 Coefficient of drag 95-percent uncertainty
(C_D scale = 0.05, $U_{95\%}C_D$ primary axis scale = 5 drag counts)

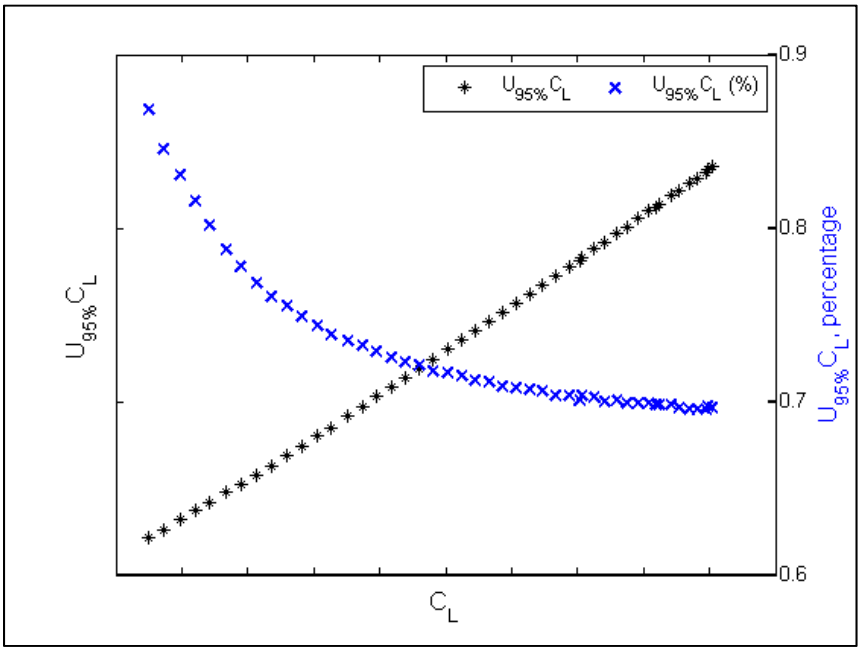

Figure 3.5 Coefficient of lift 95-percent uncertainty
(C_L scale = 0.2, $U_{95\%}C_L$ primary axis scale = 0.005)

In order to evaluate the behavior of the developed uncertainty analysis algorithm, comparisons have been made between tests with different model configurations as well as different operating conditions. Data presented in Figures 3.6 to 3.9 correspond to two runs under similar operating conditions, namely, Mach number of 0.2 and Reynolds number per foot of 8.4 million. However, the two model configurations differ in tail incidence and ice shapes. Despite the variation in aerodynamic performance of the two test articles demonstrated by Figure 3.6 and Figure 3.8, the observed uncertainties are almost identical at any given value of C_D or C_L as seen in Figure 3.7 and Figure 3.9 which in fact validates the consistency of the uncertainty analysis algorithm. Similarity in C_D or C_L under the same operating pressures indicates that the test articles are experiencing similar aerodynamic forces. Since force and pressure proved to have the largest contributions to the overall uncertainty (see section 3.2), with similar measurements of the two variables the algorithm should indeed generate similar results.

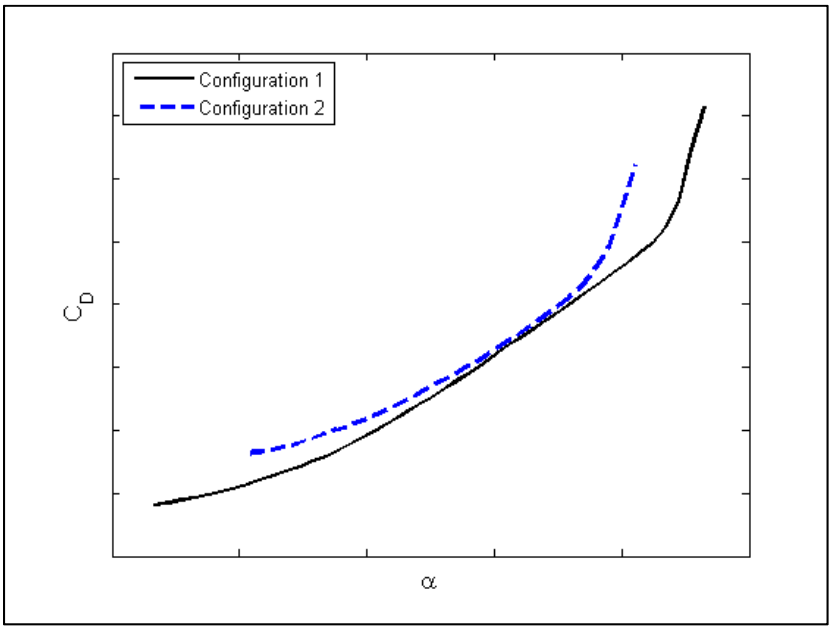

Figure 3.6 Coefficient of drag of two different model configurations tested under similar conditions

(α scale = 5 degrees, C_D scale = 0.05)

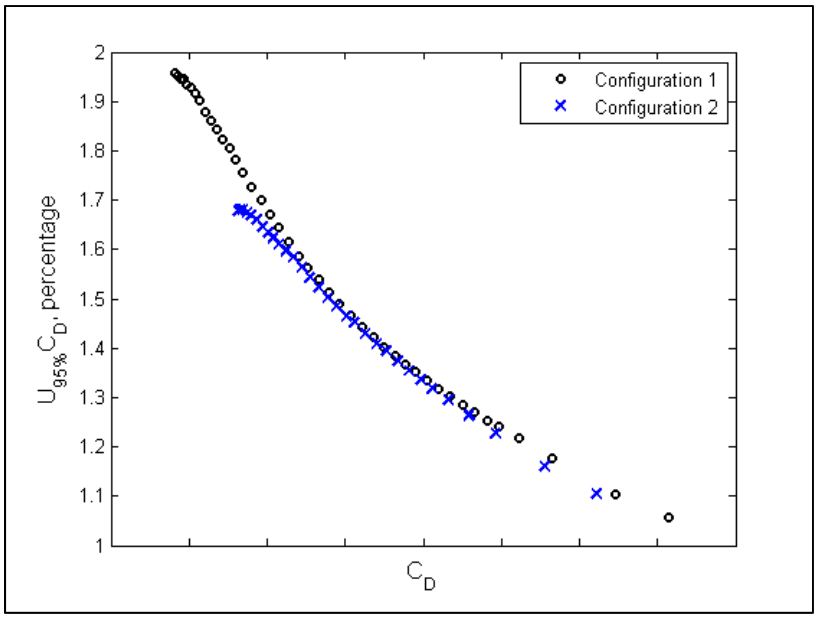

Figure 3.7 Coefficient of drag 95-percent uncertainty comparison between two different model configurations tested under similar wind tunnel operating conditions

(C_D scale = 0.05)

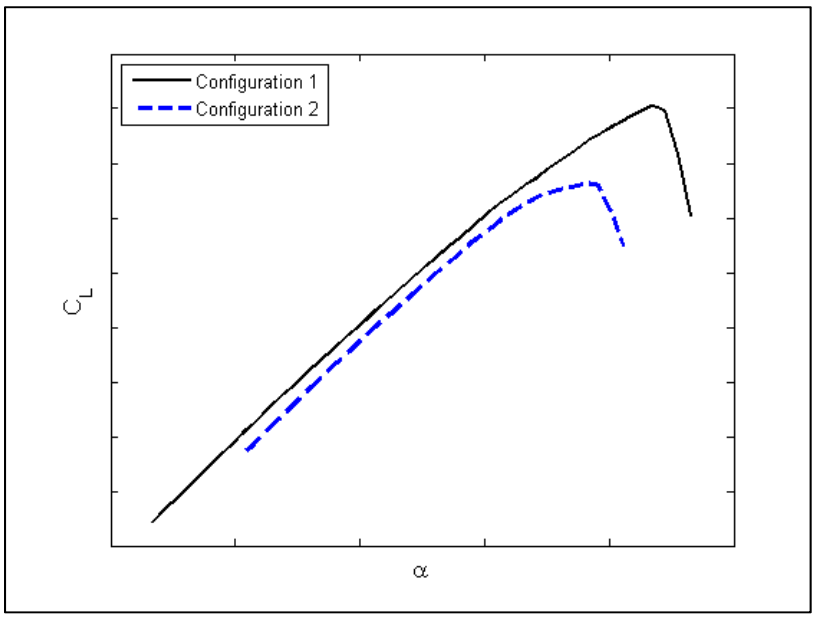

Figure 3.8 Coefficient of lift of two different model configurations tested under similar conditions

(α scale = 5 degrees, C_L scale = 0.2)

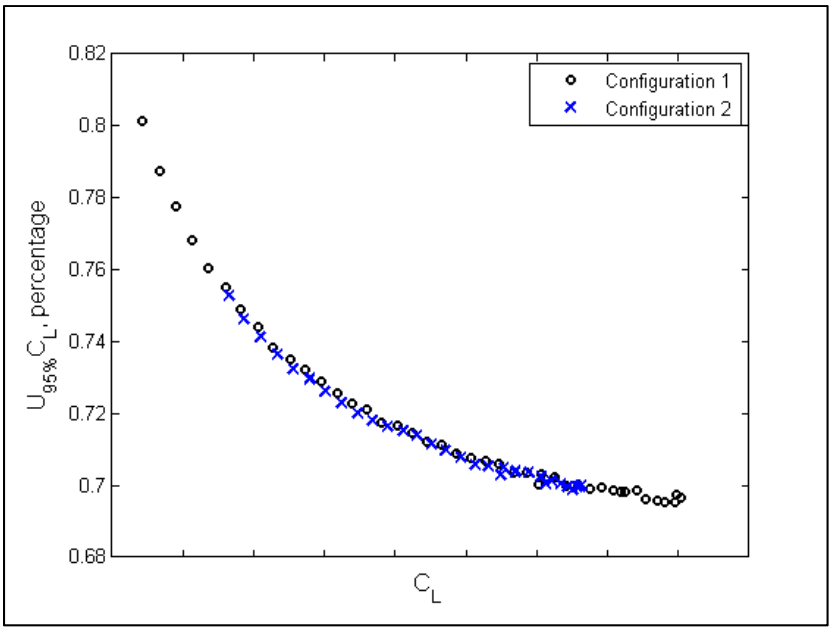

Figure 3.9 Coefficient of lift 95-percent uncertainty comparison between two different model configurations tested under similar wind tunnel operating conditions

(C_L scale = 0.2)

The effect of tunnel operating conditions on uncertainty levels is next examined by comparing the analysis results of a test with nominal Mach number of 0.2 and Reynolds number per foot of 8.4 million with those of a Mach 0.85 and Reynolds 6.2 million per foot test for the same model configuration. As illustrated by Figure 3.10 and Figure 3.11, the 95-percent uncertainties of the coefficients of drag and lift are larger in the lower Mach number test. This observation can be explained mathematically by comparing the magnitude of the terms in Eq. (2.3) and Eq. (2.5). With the measurements of the two tests being examined, the terms involving derivatives with respect to the five force components have the largest contribution to the overall uncertainties. However, those derivatives are strong functions of stagnation and freestream pressures. Since pressure levels are higher at the lower Mach number test, for example 90.9 and 88.4 psi at Mach 0.2 as opposed to 21.3 and 13.3 psi at Mach 0.85, the calculated uncertainties are consequently larger for the same measured C_D or C_L.

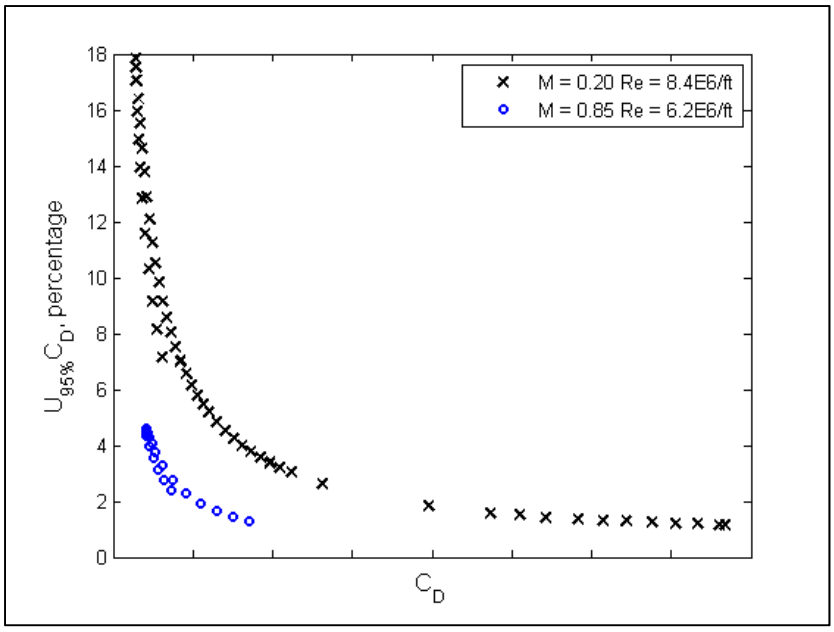

Figure 3.10 Coefficient of drag 95-percent uncertainty
at different operating conditions

(C_D scale = 0.05)

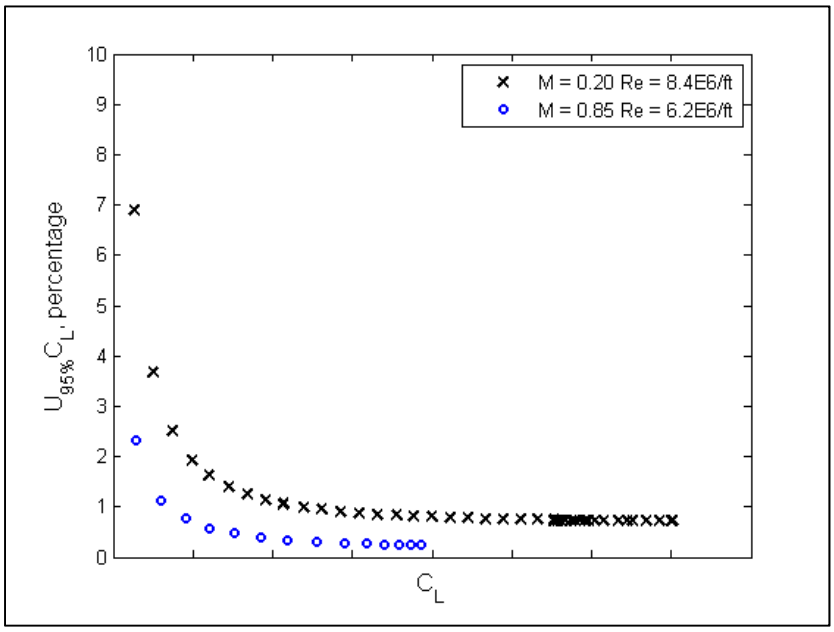

Figure 3.11 Coefficient of lift 95-percent uncertainty
at different operating conditions

(C_L scale = 0.2)

The effect of the freestream properties on the force and moment coefficient uncertainties is further assessed using the data obtained from a particular model configuration that was tested under the most number of nominal test conditions. Figure 3.12 presents the result for C_D as an example which reveals that the 95-percent uncertainty is lower at higher Mach number tests, for any given model attitude. The trend is consistent with the result of a similar analysis at the NASA Marshall Space Flight Center trisonic wind tunnel (Springer, 1999). It should be emphasized that the reported test section Mach numbers are achieved at the pressure levels specific to the Bombardier experiments, which were summarized in Table 1.1. The trend may alter if the desired Mach is obtained using a different combination of stagnation and static pressures having the same ratio as those of Table 1.1.

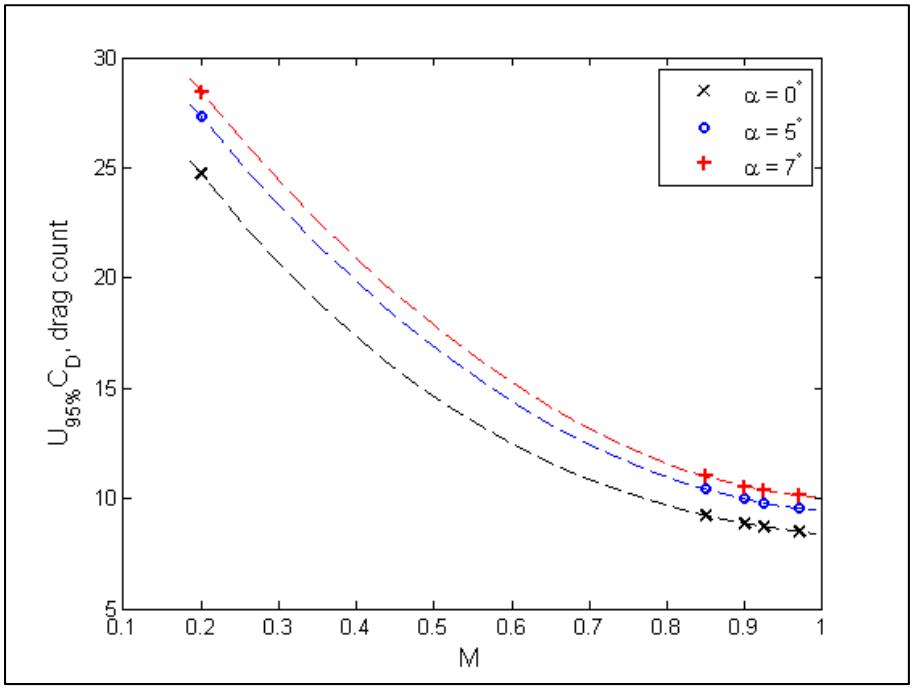

Figure 3.12 Coefficient of drag 95-percent uncertainty at different Mach numbers

(Curve fits are only for illustration purposes to highlight the trend)

The uncertainty of the freestream parameters such as the calculated test section Mach number and dynamic pressure have also been examined using the measurements of stagnation and freestream pressures of a sample run at every common operating condition of the Bombardier

half-model experiments. The analysis results are presented in Figure 3.13 and Figure 3.14 in both absolute value and percentage. Even though the pressure measurements vary slightly during a run, and also from one run to another at a given nominal operating condition, the calculated uncertainties are essentially constant throughout a run, and also identical for all the runs with the same nominal Mach or dynamic pressure. Hence, Figure 3.13 and Figure 3.14 represent general uncertainties over the entire operating range of the half-model experiments. The low levels of total uncertainties in these freestream properties indicate that the desired test conditions are achieved with very high accuracy at the NRC wind tunnel.

The estimated Mach number and dynamic pressure uncertainties are of the same order of magnitude as those obtained by Springer (1999) at the NASA Marshall Space Flight Center, and also by Ulbrich and Boone (2004) at the NASA Ames Research Center, under similar test conditions.

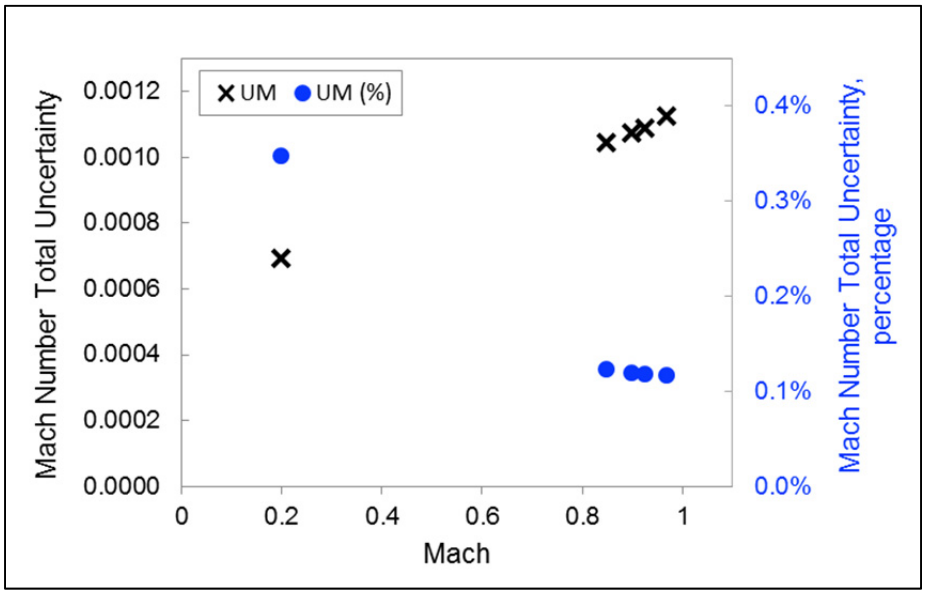

Figure 3.13 Test section freestream Mach number 95-percent uncertainty
(Presented as absolute value on the primary axis and as percentage of the nominal Mach on the secondary axis)

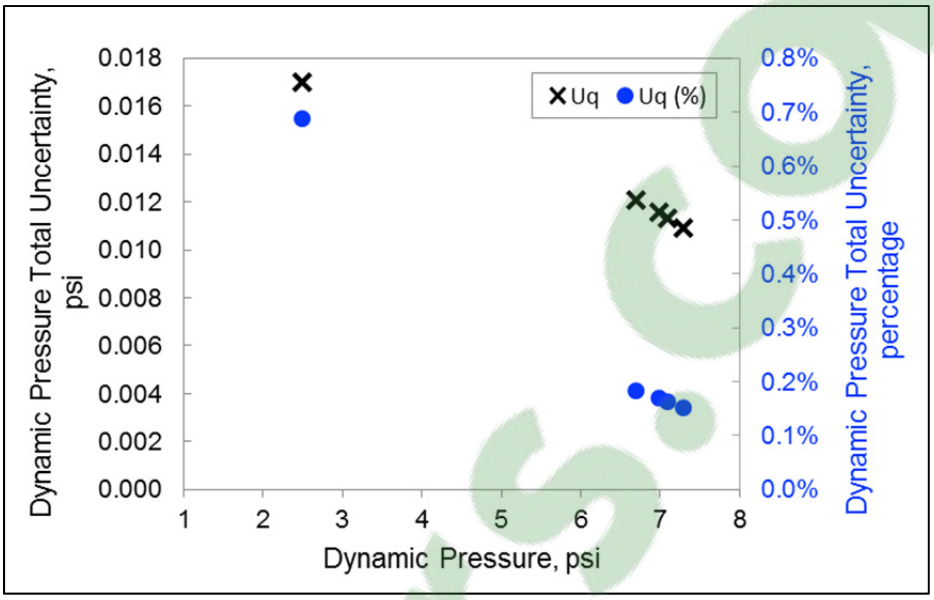

Figure 3.14 Test section freestream dynamic pressure 95-percent uncertainty

(Presented as absolute value on the primary axis and as percentage of the nominal dynamic pressure on the secondary axis)

3.2 Uncertainty Breakdowns

It is insightful to separately examine the systematic and random components of the total 95-percent uncertainty. Examples of such breakdown are presented in Figure 3.15 and Figure 3.16 for the coefficient of drag and the coefficient of lift, respectively, at selected values of angles of attack during a low speed run. The analysis clearly indicates that the inherent bias error of the measurement system, estimated by the systematic uncertainty, is of the same order of magnitude as the precision error or the random uncertainty, and should not be overlooked when considering the data quality. The relative magnitudes of the two components change with tunnel conditions and from one test article to another. In the provided example, the total uncertainty of C_D is mostly dominated by systematic errors while that of C_L is most affected by random errors. Note that the increasing trend in the calculated systematic, random and total uncertainties is associated with the increase in C_D and C_L or the measured forces during the angle sweep, as discussed previously.

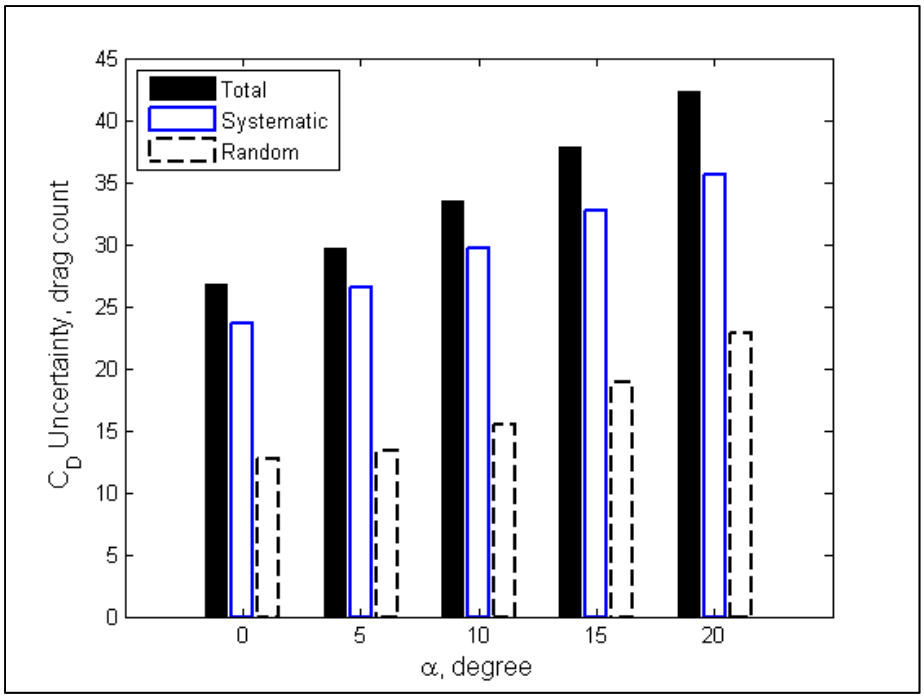

Figure 3.15 Systematic, random and total 95-percent uncertainty of coefficient of drag

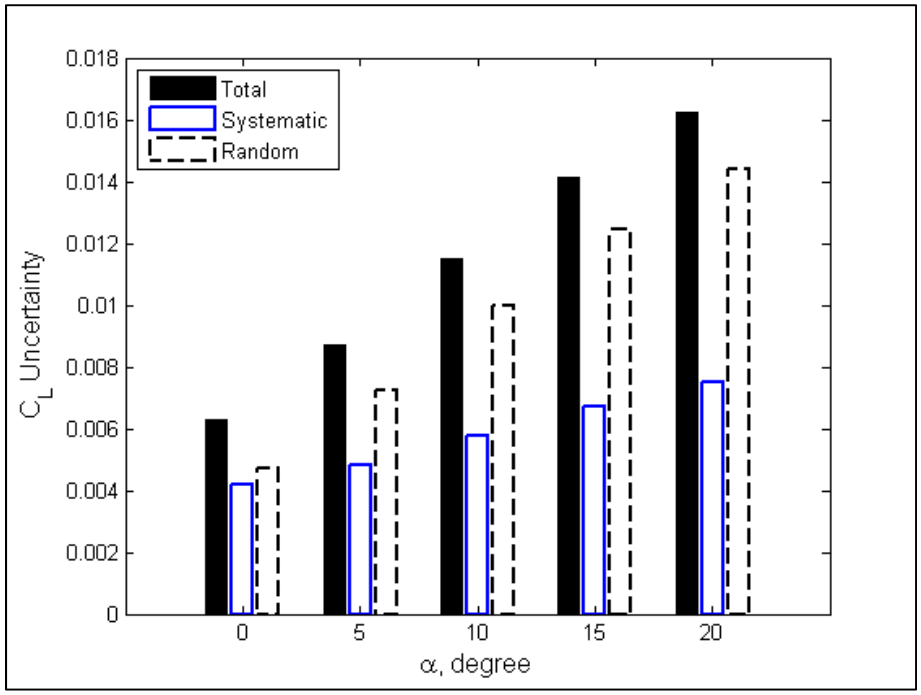

Figure 3.16 Systematic, random and total 95-percent uncertainty of coefficient of lift

Another valuable breakdown of total uncertainty is obtained by separating the contribution of each independent variable to the overall calculated uncertainties. Following the methodology explained in section 2.1, the contribution of variable x_i is defined as

$$U_i = \sqrt{\left(\frac{\partial r}{\partial x_i} s_i\right)^2 + \left(\frac{\partial r}{\partial x_i} b_i\right)^2 + 2\frac{\partial r}{\partial x_m}\frac{\partial r}{\partial x_n} b'(x_m, x_n)} \tag{3.1}$$

For the force contribution, Eq. (3.1) involves precision and bias limits of all five balance elements, and also the correlated bias errors among the pairs. The pressure contribution is obtained as the sum of the contributions of stagnation and freestream pressure, namely their precision and bias limits and a correlated bias error term. It should be noted that the component uncertainties combine as root-sum-squares. Hence, the uncertainty percentage contribution or UPC of each independent variable to the total uncertainty of a result parameter is defined as

$$\text{UPC}_i = \frac{U_i^2}{U_r^2} \times 100 \tag{3.2}$$

(Coleman and Steele, 2009; Stephens et al, 2016). Figure 3.17 and Figure 3.18 illustrate the UPC of the most significant variables to the total uncertainties of C_D and C_L at selected angles of attack for a low speed run. *F* contribution represents the combined effect of the five force measurements of the balance, while *P* represents the combination of stagnation and freestream pressure contributions. In this example, the force components have the largest contribution to the overall uncertainty of C_D while that of C_L is mostly affected by pressure. The UPC of the angle of attack to C_L uncertainty is not significant in the example of Figure 3.18, and is therefore not shown on the graph.

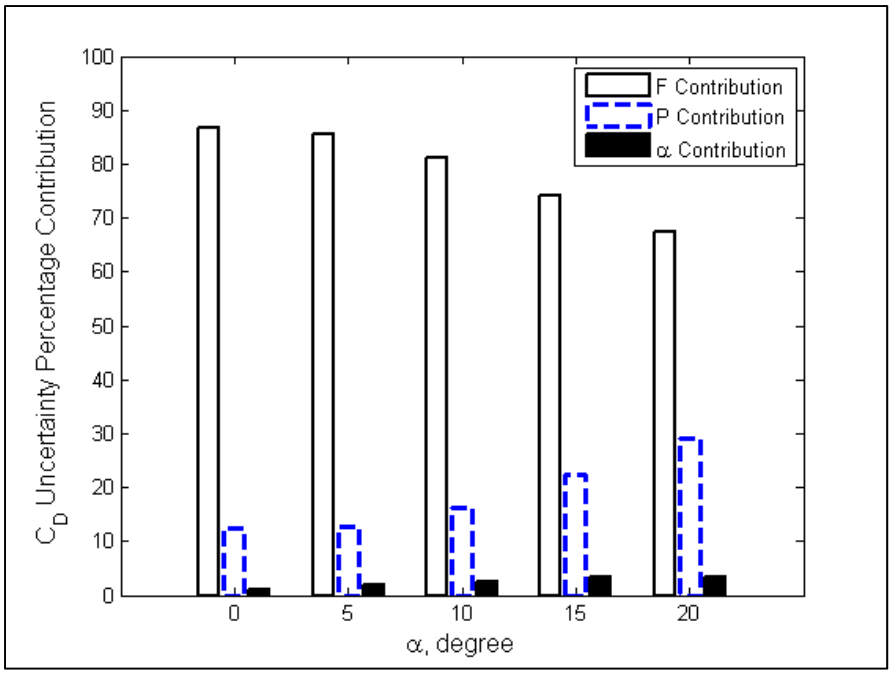

Figure 3.17 Breakdown of contributions for coefficient of drag total uncertainty

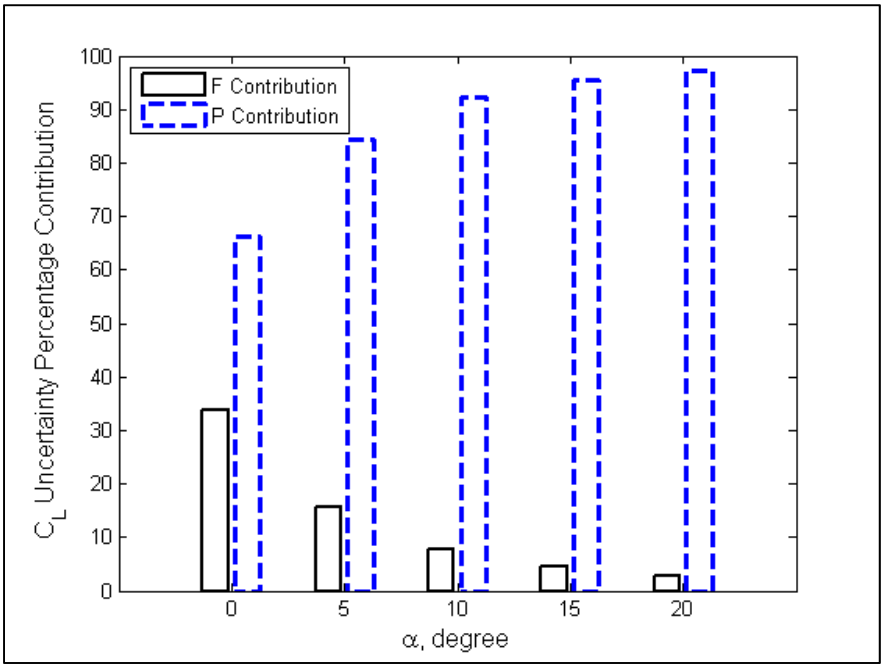

Figure 3.18 Breakdown of contributions for coefficient of lift total uncertainty

It should be noted that the percent contribution of the variables to the total uncertainty of the result parameters vary not only with the angle of attack during a run, but also from one run to another. For example, Figure 3.19 shows the percent contributions of the force and pressure components to the overall uncertainty of C_L in another low speed run, where the test article had different tail incidence, flap design, and slat deflection angle than that of the run analyzed for Figure 3.18. The two model configurations were tested under the same operating conditions, namely, nominal Mach number of 0.2 and Reynolds number per foot of 8.4 million. Hence, the measured stagnation and freestream pressure are similar in the two runs. However, as the two models exhibit distinct aerodynamic performances, the measured forces during these two runs are different. Consequently, the magnitudes of the partial derivatives of Eq. (3.1) are overall different for the two runs, which result in unique UPC breakdowns for the uncertainty of C_L, or any other force or moment coefficient, for each run. The fact that the percentage contributions vary with the angle of attack during a run is also explained simply by the change in the magnitudes of the partial derivatives involved in the UPC calculations, as the force measurements change with α.

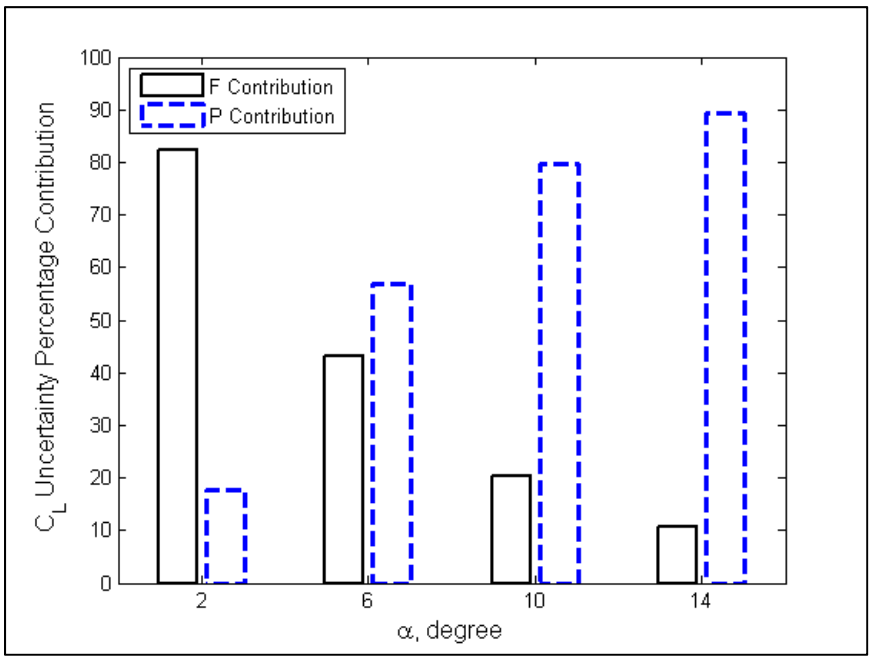

Figure 3.19 Breakdown of contributions for coefficient of lift total uncertainty of an alternative model configuration at low speed condition

Another example of UPC variation is provided by Figure 3.20, for which data are obtained by testing the model configuration of Figure 3.19 under a high speed condition, namely Mach 0.85 and Reynolds 6.2 million per foot. The stagnation and freestream pressure measurements in a low speed test are around 90.9 and 88.4 psi respectively, while those of a Mach 0.85 test are around 21.3 and 13.3 psi. Besides, since the model performs differently under the two test conditions, the forces measured during the two runs are also different. Consequently, with distinct force and pressure data, the calculated partial derivatives and ultimately the uncertainty percentage contribution of the force and pressure components to the overall uncertainty of C_L of the two runs are inevitably different. The variation is even more pronounced if one compares runs with different model configurations and operating conditions. While in the run presented in Figure 3.18 pressure has the most significant contribution to the overall uncertainty of C_L, force appears to be the major contributing factor to that of C_L in the run shown in Figure 3.20.

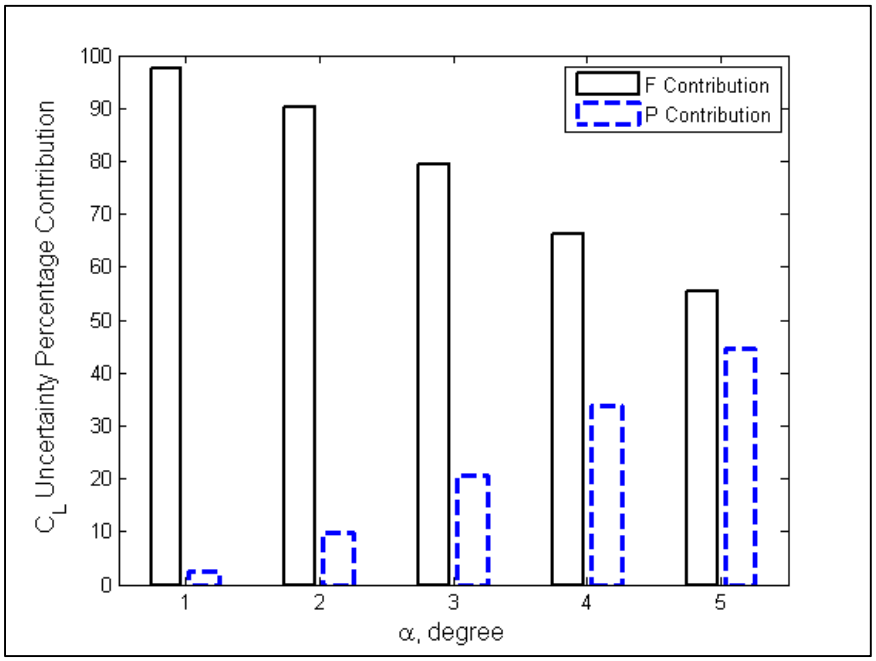

Figure 3.20 Breakdown of contributions for coefficient of lift total uncertainty of an alternative model configuration at high speed condition

Even though the percentage contribution of the independent variables to the uncertainties vary during a run and also with the tunnel condition and from one test article to another, force and pressure measurements consistently have the two largest contributions to the overall calculated uncertainties of all the resultant force and moment coefficients. Therefore, the analysis recommends that the NRC tunnel can most benefit from an increase in the measurement accuracy of the half-model balance and the P_0 and P_I pressure transducers if a lower data uncertainty is desired.

Since random errors are assumed to be uncorrelated (AIAA, 1999; Coleman and Steele, 2009), the contribution of pressure and force to the random portion of the total uncertainty can be further broken down to the individual component level. In this case, the percentage contribution is computed by considering only the precision terms in Eq. (3.1) and Eq. (3.2). The new expression becomes of the form

$$\text{Random UPC}_{x_i} = \frac{\left(\frac{\partial r}{\partial x_i} s_i\right)^2}{S_r^2} \times 100 \tag{3.3}$$

for the percentage contribution of the independent variable x_i to the 95-percent random uncertainty of a result parameter r. Hence, when addressing the total random uncertainty, instead of a combined force component, the effects of balance axial force components X_1 and X_2, and normal force components N_1, N_2 and N_3 may be investigated separately. Similarly, the pressure component can be expressed in terms of separate stagnation pressure P_0, and freestream pressure P_I contributions to the overall random uncertainty. Figure 3.21 and Figure 3.22 show the UPC of the most significant measured variables to the random uncertainties of C_D and C_L at selected angles of attack, for one of the analyzed low speed runs. In this example, the balance axial force components have the largest percentage contribution to the overall random uncertainty of C_D, followed by the stagnation pressure. On the other hand, the stagnation pressure is the largest contributor to the random uncertainty of C_L. At low angle of attack, the three normal force components also contribute to the random

uncertainty of C_L but the effect of pressure terms dominates at high α. Hence, reducing the precision error of the balance and the stagnation pressure measurements would have the largest impact on the variability of C_D and C_L.

The study conducted by Walter, Lawrence and Elder at the National Transonic Facility (2010) also shows that force elements have the largest contribution to the total uncertainty of C_D, followed by dynamic pressure which reflects the combined effect of stagnation and static pressure uncertainties, and next the model pitch and roll angles. Similarly, Kammeyer (1999) reveals that axial force and total pressure are the top two contributing factors to the uncertainty of C_D at the Naval Surface Warfare Center hypervelocity wind tunnel.

It should be emphasized again that the relative magnitudes of the contribution of the independent variables to the total or the random uncertainties vary with the operating conditions and from one test article to another. However, with the current estimates of the bias and precision limits and for the analyzed runs, force and pressure components proved to be the most significant contributing factors to the uncertainties of C_D and C_L.

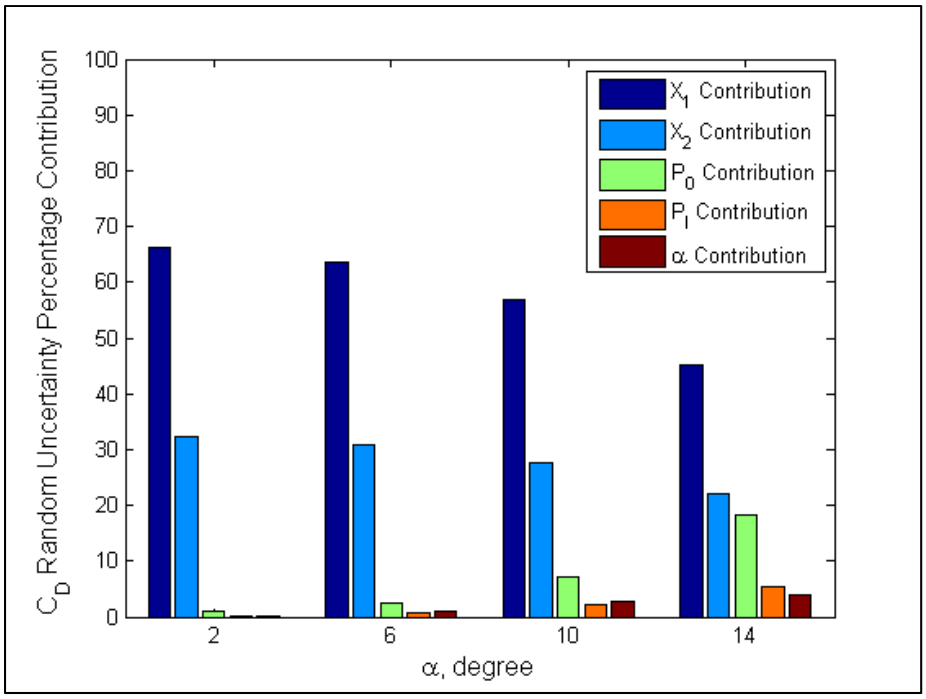

Figure 3.21 Breakdown of contributions for coefficient of drag random uncertainty

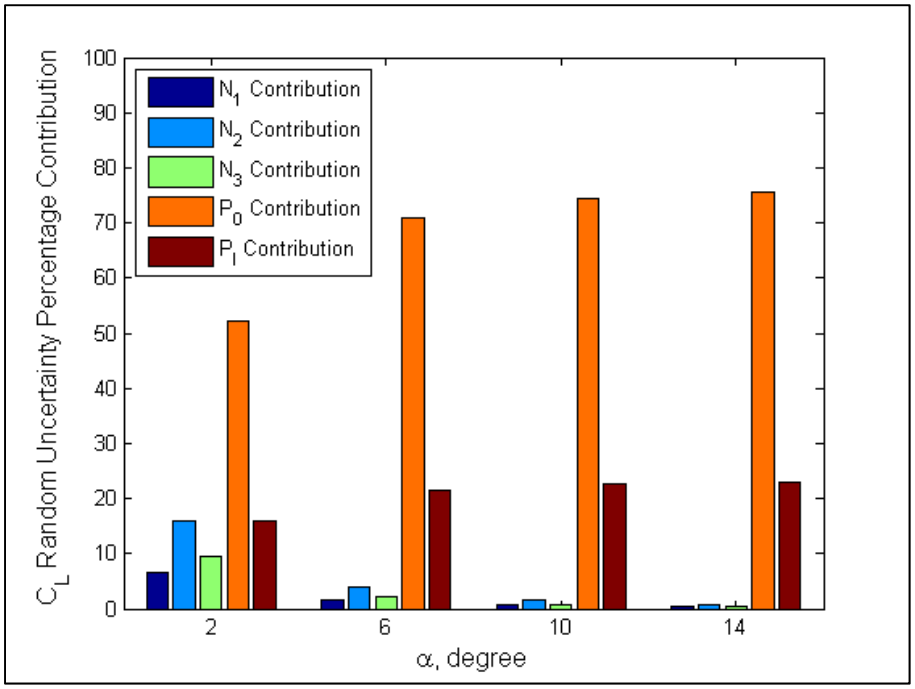

Figure 3.22 Breakdown of contributions for coefficient of lift random uncertainty

The analysis has been also performed on the calculated test section Mach number and dynamic pressure in order to obtain their respective uncertainty breakdowns. Figures 3.23 and 3.24 present the systematic and random components of Mach number and dynamic pressure uncertainties at the common operating conditions which combine as root-sum-square to yield total 95-percent uncertainties. It is evident again that the effect of the bias errors of the measurement system, represented by the systematic uncertainty, can be of the same order of magnitude as that of the precision errors reflected in the random uncertainty. Hence, the bias and the precision errors deserve equal attention in the estimation of the overall data quality at the NRC tunnel. Stephens et al. (2016) emphasize as well on the importance of fully understanding and accounting for all the bias error sources, as they express that the total uncertainty in Mach number is strongly driven by systematic uncertainty at the NASA Glenn wind tunnel. Springer (1999) also reveals that the bias errors dominate the uncertainty of Mach number and dynamic pressure at the NASA Marshall Space Flight Center trisonic wind tunnel and should not be overlooked. Notably, the estimated random uncertainties of both Mach number and dynamic pressure are of the same magnitude as those obtained by Walter et al. at the National Transonic Facility transonic wind tunnel when compared under similar test conditions (Walter, Lawrence and Elder, 2010).

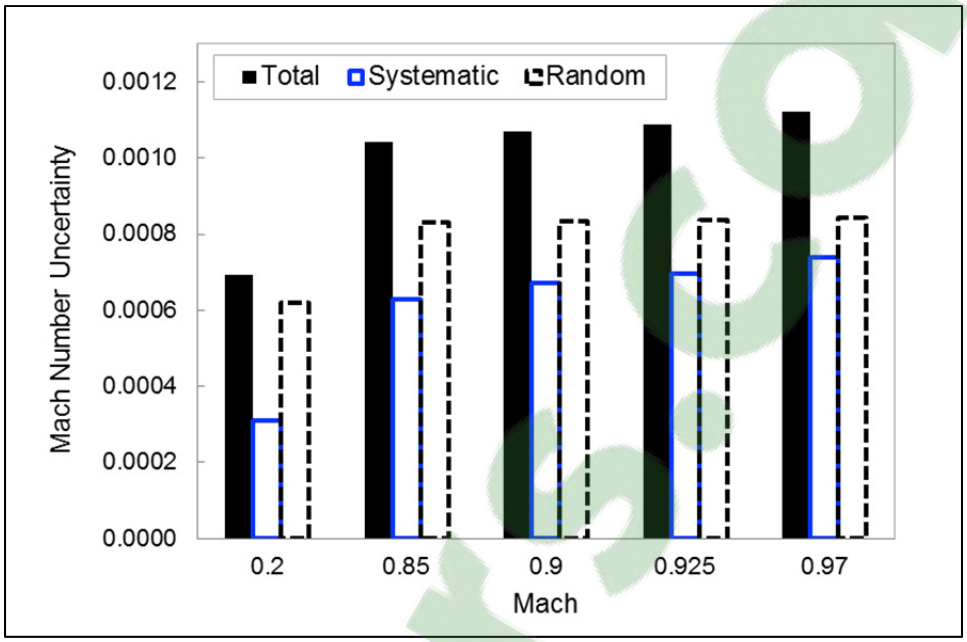

Figure 3.23 Systematic, random and total 95-percent uncertainty of Mach number

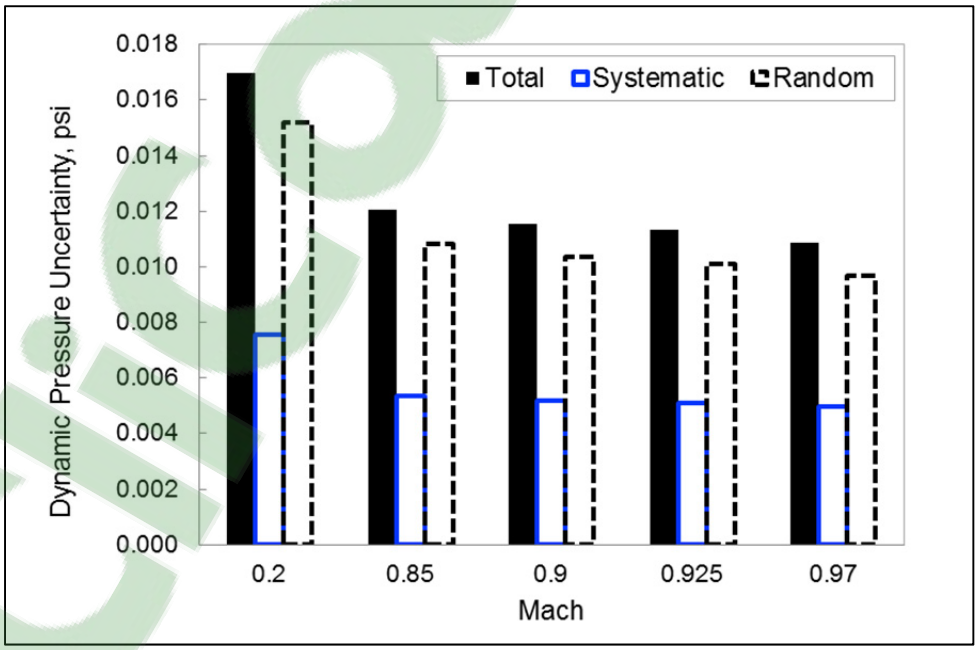

Figure 3.24 Systematic, random and total 95-percent uncertainty of dynamic pressure

As seen in Eq. (2.8) and Eq. (2.9), the independent variables involved in the expressions of Mach number and dynamic pressure are the stagnation and static pressures, P_0 and P_I. Therefore, a breakdown of the 95-percent total uncertainties of Mach and dynamic pressure would only indicate 100% contribution by pressure. The random uncertainty however can be broken down to separate P_0 and P_I contribution components, as shown in Figure 3.25 and Figure 3.26 for Mach number and dynamic pressure respectively. With the current estimates of the precision limits, the stagnation pressure has a more significant contribution to the random uncertainty of these two freestream parameters, especially in the case of dynamic pressure. Hence, reducing the precision error in the measurements of stagnation pressure would have the largest impact on the overall variability of these freestream properties.

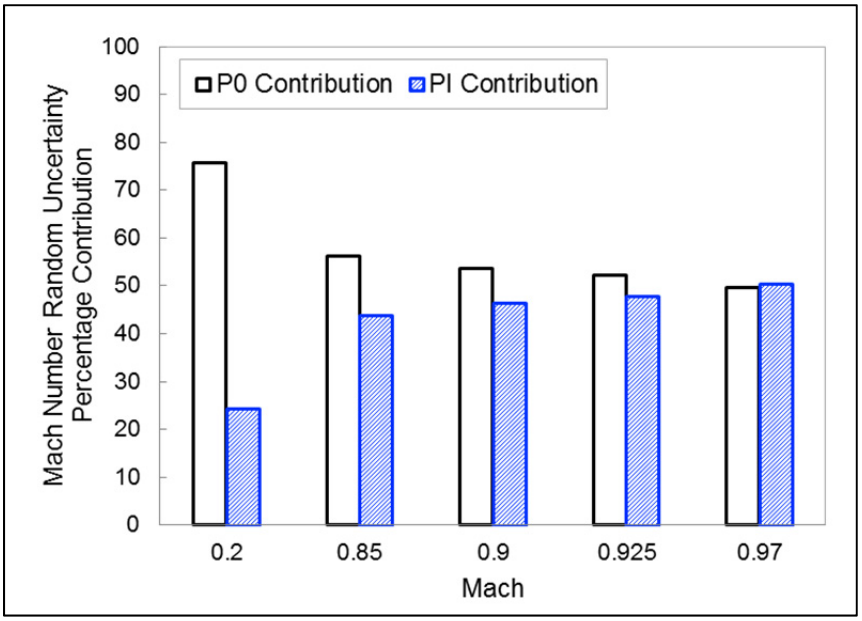

Figure 3.25 Breakdown of contributions for Mach number random uncertainty

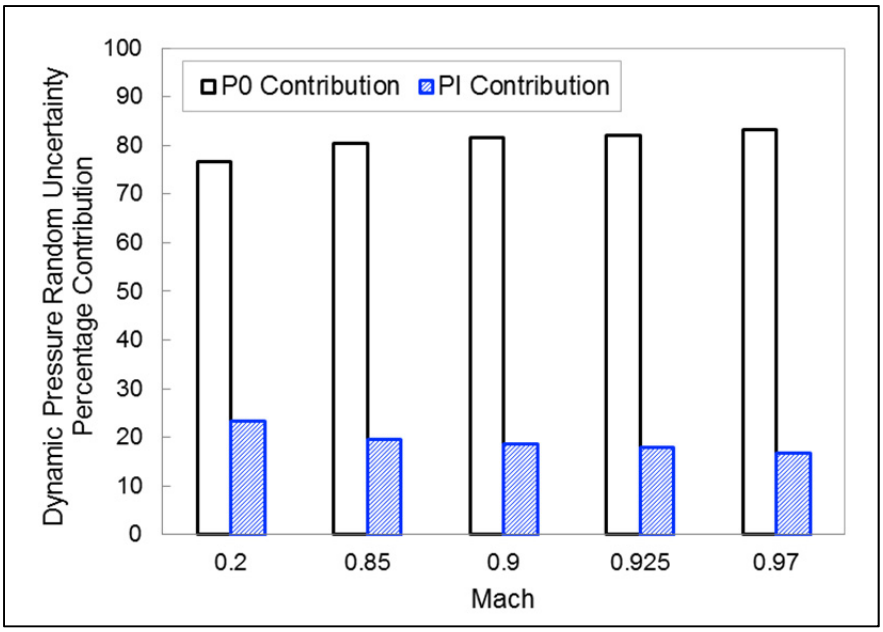

Figure 3.26 Breakdown of contributions for dynamic pressure random uncertainty

3.3 Validation

In order to validate the developed algorithm and the TSM uncertainty calculations, an alternative Monte Carlo method of uncertainty propagation has been carried out for the same system. In this method, a distribution of possible values for each result parameter is obtained through an iterative offline simulation of the data reduction equations, and the standard deviation of this generated distribution is an estimate of the total uncertainty of the parameter (Coleman and Steele, 2009). Figure 3.27 illustrates the Monte Carlo simulation steps for a data reduction equation involving two independent variables x_1 and x_2 as an example. A Gaussian distribution is assumed for the bias and precision errors of every independent variables, centered at zero, with a standard deviation equivalent to half of the corresponding estimated bias and precision limits. At every step of the simulation, a random number generator is used to select an error value from each distribution. These values are then added to the measured value of the relevant independent variables and the result parameter is calculated using the data reduction equations. The same sampled error value is used for the variables whose bias errors are believed to be correlated (Coleman and Steele, 2009). This

process is repeated 100,000 times for the tunnel freestream parameters and all the force and moment coefficients to obtain a Gaussian distribution of possible values for each. The standard deviation of the result distributions, with a coverage factor of 2 corresponding to a 95-percent confidence interval, is an estimate of the total uncertainty of the parameter (Coleman and Steele, 2009).

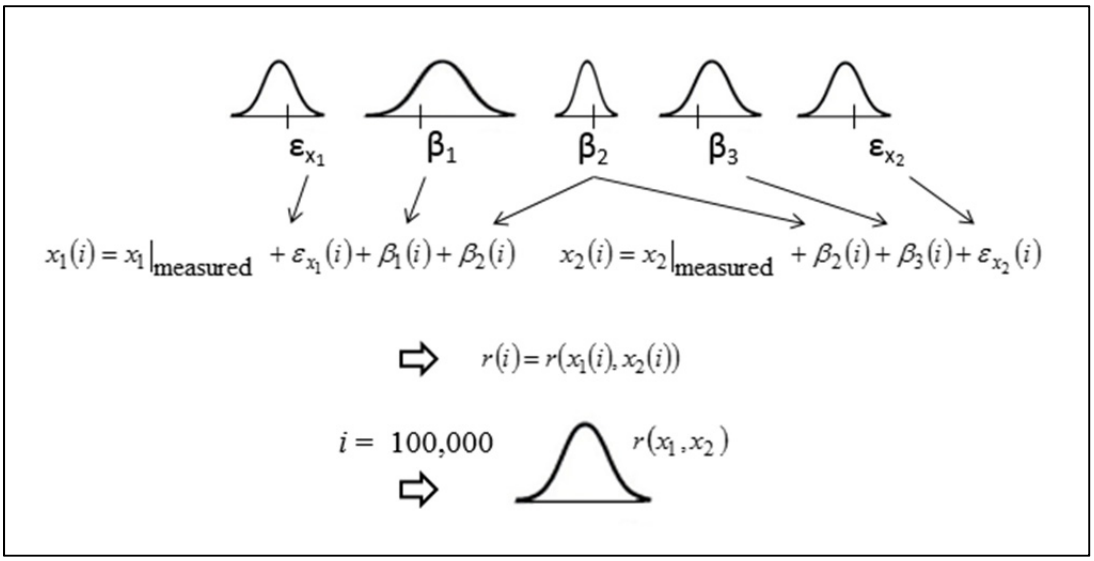

Figure 3.27 Monte Carlo simulation process (adapted from Coleman and Steele, 2009)

The total uncertainties obtained through MCM propagation are within 10 percent of those obtained through TSM propagation. This range is believed to be reasonable for validation purposes, given the inherent differences in how the two methods account for the correlated bias errors. When the MCM analysis is carried out with only the random errors, which are assumed to be uncorrelated, the 95-percent random uncertainty estimates obtained by the two methods agree within one percent for Mach number, dynamic pressure and all the force and moment coefficients. This validates the mathematics and the implementation of the developed uncertainty analysis algorithm. The difference between the TSM and MCM estimations of the total uncertainties in Mach number, dynamic pressure, coefficient of lift and coefficient of drag are presented in Figure 3.28, while Figure 3.29 presents the difference in the estimates of the random uncertainties, for one of the analyzed low speed runs. The values are reported in percent difference relative to the TSM estimates.

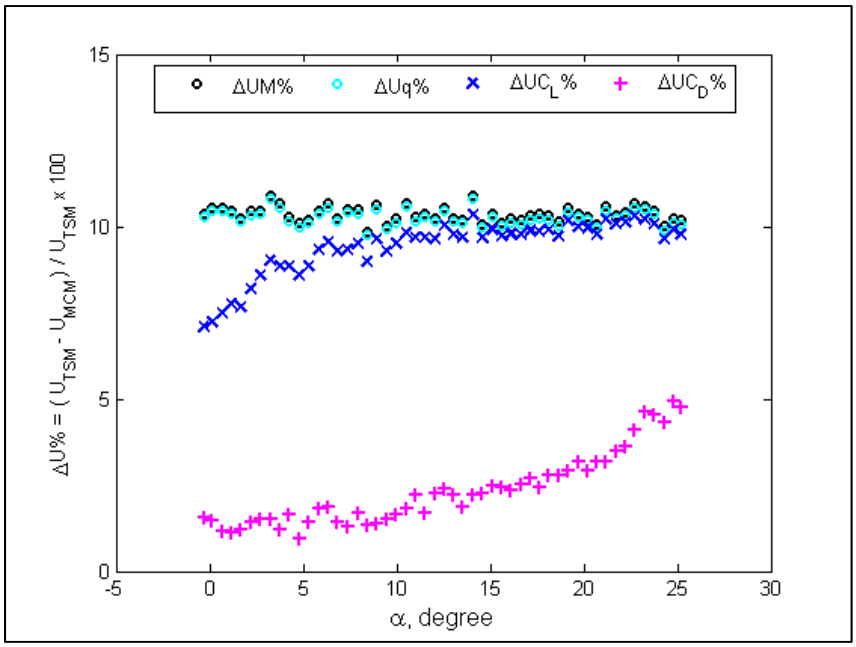

Figure 3.28 Comparison of TSM and MCM estimates of total uncertainties

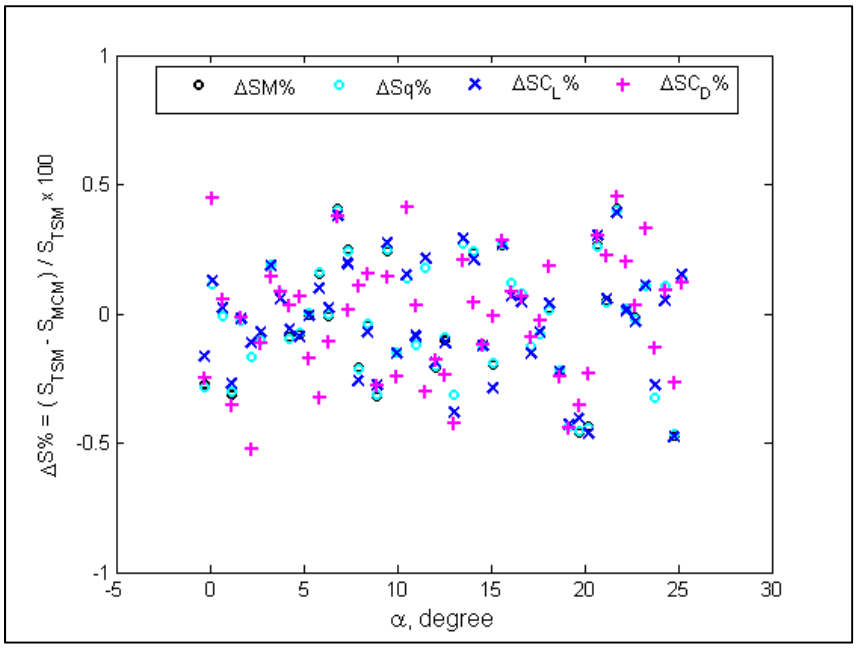

Figure 3.29 Comparison of TSM and MCM estimates of random uncertainties

The increasing trend in the C_L and C_D validation curves of Figure 3.28 corresponds to the increase in force measurements with the angle of attack, or equivalently to the increase in C_L and C_D, which consequently increases the effects of the correlated bias errors of the measurements on the calculated uncertainties. Hence, the discrepancy between the TSM and MCM estimates of the uncertainties also escalates with the angle of attack, as the correlated bias error terms are accounted for differently in the two methods. In TSM calculations, a covariance term is calculated for every pair of variables whose bias errors are believed to be correlated due to calibration of their respective measurement devices against a common working standard, as expressed by Eq. (2.5) and Eq. (2.6). The uncertainty of the working standard U_{ws} is used as the bias limit of the common elemental error source in Eq. (2.6). For example, the covariance term for the correlated bias error of the stagnation and the freestream static pressure measurements P_0 and P_I is calculated as

$$b'(P_0, P_I) = (U_{ws})_{P_0} \times (U_{ws})_{P_I} = 0.0044 \times 0.0044 = 1.94 \times 10^{-5}\ \text{psi}^2 \tag{3.4}$$

and the corresponding correlated bias error term in Eq. (2.5) for every result parameters r, at every measurement point, is of the form

$$2 \frac{\partial r}{\partial P_0} \frac{\partial r}{\partial P_I} b'(P_0, P_I) \tag{3.5}$$

Besides, separate bias error terms are calculated for P_0 and P_I in Eq. (2.5), which allows distinct bias limits to be assigned to the measurements of the two pressures, aside from the correlated bias value. On the other hand, in MCM calculations the effect of the correlated bias errors are represented by assigning the same bias value, which is randomly selected from the corresponding error distribution at every step of the simulation, to the measurements of all the variables whose bias errors are assumed to be correlated. Hence, only a single bias error distribution can be considered for such variables. For example, in the validation study, the bias error in P_0 and P_I measurements is assumed to be distributed around the uncertainty of the common working standard, and at every iteration the same error value selected by the

random generator from this distribution is added to the measured values of both P_0 and P_I in order to represent the combined contribution of their measurement bias to the systematic uncertainty of the results. As the estimated bias limits of P_0 and P_I are indeed different and higher than the uncertainty of the working standard used in their calibration, the TSM technique of accounting for the bias errors is presumably more accurate.

Due to the explained inherent differences in the TSM and MCM propagation of the bias errors, the total uncertainties in the freestream properties and the force and moment coefficients calculated by the two methods are inevitably different, and the level of agreement observed in Figure 3.28 is deemed reasonable for validation purposes. As seen in Figure 3.29, the random uncertainty estimates of the two methods are essentially identical, which confirms that the observed discrepancy between the TSM and MCM total uncertainties of Figure 3.28 is rooted in the treatment of the bias correlations, since the random errors are assumed to be uncorrelated (AIAA, 1999; Coleman and Steele, 2009). Consequently, the mathematics and the implementation of the developed uncertainty algorithm are validated through this alternative error propagation methodology. Even though the MCM analysis appears to be simpler and often more practical for complicated data reduction procedures, the TSM is chosen as the preferred uncertainty model for the NRC tunnel, because of its analytical nature which works well with the straightforward non-iterative data reduction equations involved in the Bombardier half-model experiments. Moreover, the TSM algorithm can report the uncertainties instantly along with the test results, unlike the MCM approach for which the simulation has to be performed offline after the raw data are reduced.

Once the computational aspect of the analysis is validated, it is desired to assess the overall goodness of the total uncertainty estimates of the experimental results, which is in fact limited to the goodness of the bias and precision limit estimates that are propagated (Stephens et al., 2016). The focus has been on the random component of the uncertainty, since the systematic component is already the best estimate of the unknown bias of the measurement system. The calculated 95-percent random uncertainty of Mach number M and dynamic pressure q has been compared with the observed variability, represented by 2σ or

the expanded standard deviation of the measured values of the respective parameter during a number of runs under identical nominal conditions. The results are presented in Figure 3.30 and Figure 3.31 for Mach number and dynamic pressure as absolute value, while Figure 3.32 and Figure 3.33 report the results as percentage of the nominal value of the respective parameter for better comparison. The observed and calculated values at Mach 0.2, 0.85, 0.9 and 0.925, or the corresponding dynamic pressures, are averaged over 21, 12, 12 and 11 different runs respectively. Overall, given the fact that the uncertainty analysis is limited to the data reduction process and does not take into account the errors caused by variations in the tunnel operation (Walter, Lawrence and Elder, 2010), a good agreement exists between the observed and the calculated values for both parameters. Notably, the extent of the agreement or the difference between the observed variability and the calculated random uncertainty is of the same order of magnitude as that reported by Walter et al. at the National Transonic Facility (2010), where the calculated random uncertainties of these two freestream properties are obtained through an offline MCM simulation, and the observed values are estimated from numerous benchmark tests.

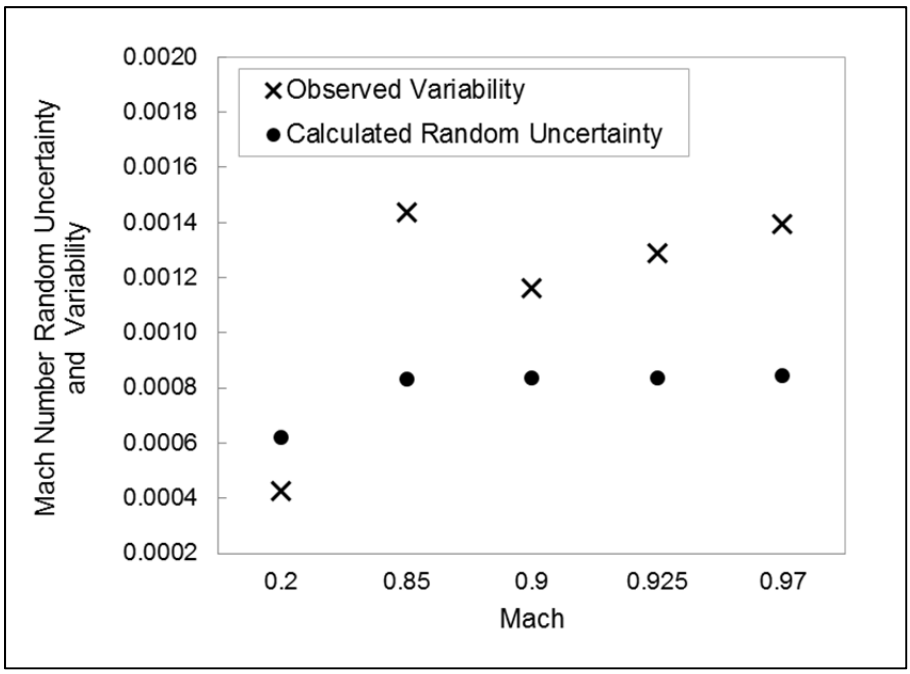

Figure 3.30 Mach number uncertainty validation

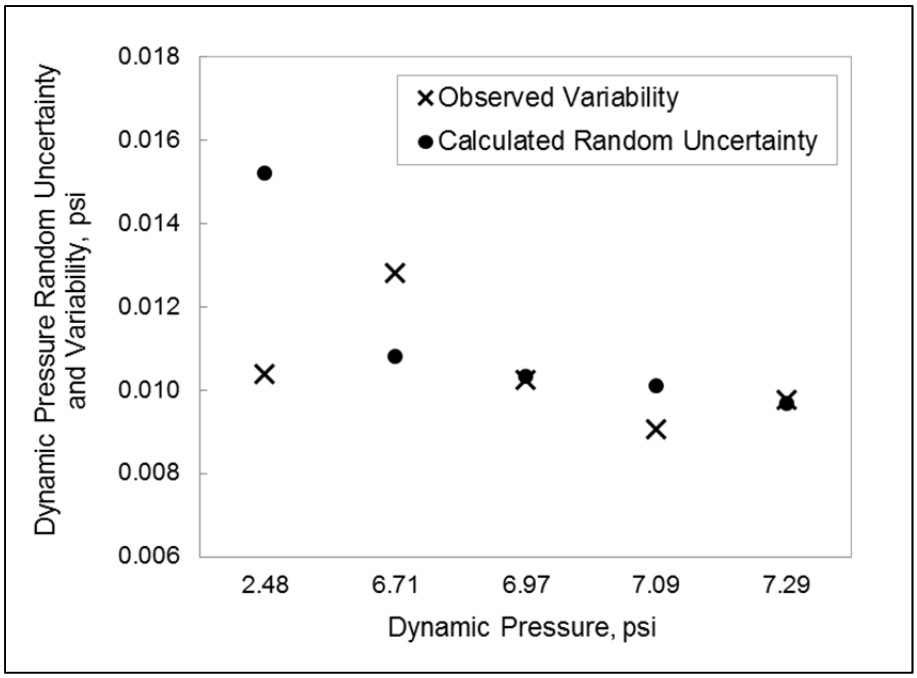

Figure 3.31 Dynamic pressure uncertainty validation

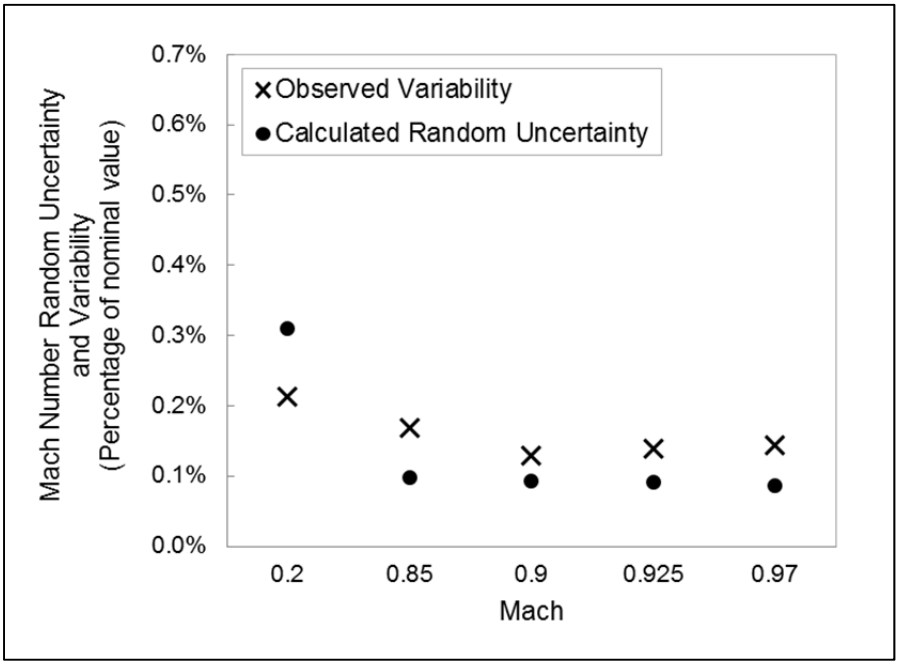

Figure 3.32 Mach number random uncertainty and observed variability as percentage of the nominal Mach

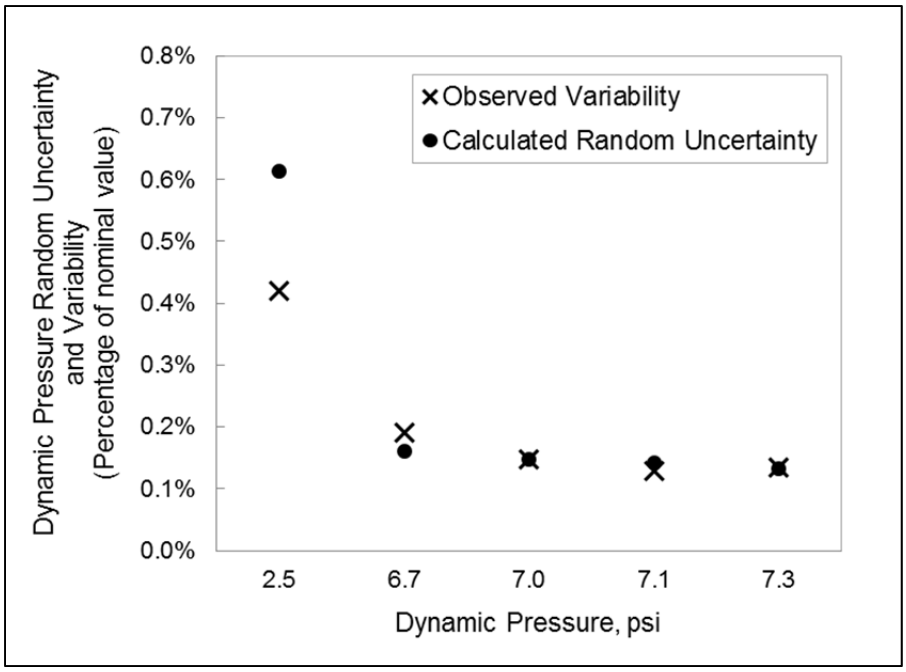

Figure 3.33 Dynamic pressure random uncertainty and observed variability as percentage of the nominal dynamic pressure

Nevertheless, it is compelling to investigate the apparent deviation at Mach 0.2 for the case of dynamic pressure. Since the expressions of the calculated Mach number and dynamic pressure are only functions of freestream and stagnation pressure, any major discrepancy between the observed and calculated values of the random uncertainty could indicate that the precision errors of the pressure measurement system are not completely accounted for in the uncertainty analysis. For instance, correlated precision or random errors are neglected in the TSM propagation, but an investigation of the two measured pressures reveals a clear trend between the random variations in their readings during a run. Figure 3.34 shows the measured values of stagnation and static pressures during a low speed run as an example, and Figure 3.35 highlights the observed trend in their variation which suggests that a correlation exists between the random errors of these two variables (Stephens et al., 2016). Not accounting for these correlated errors overestimates the random uncertainty of the result parameters (Coleman and Steele, 2009; Stephens et al., 2016), especially under low speed conditions where pressure levels are higher.

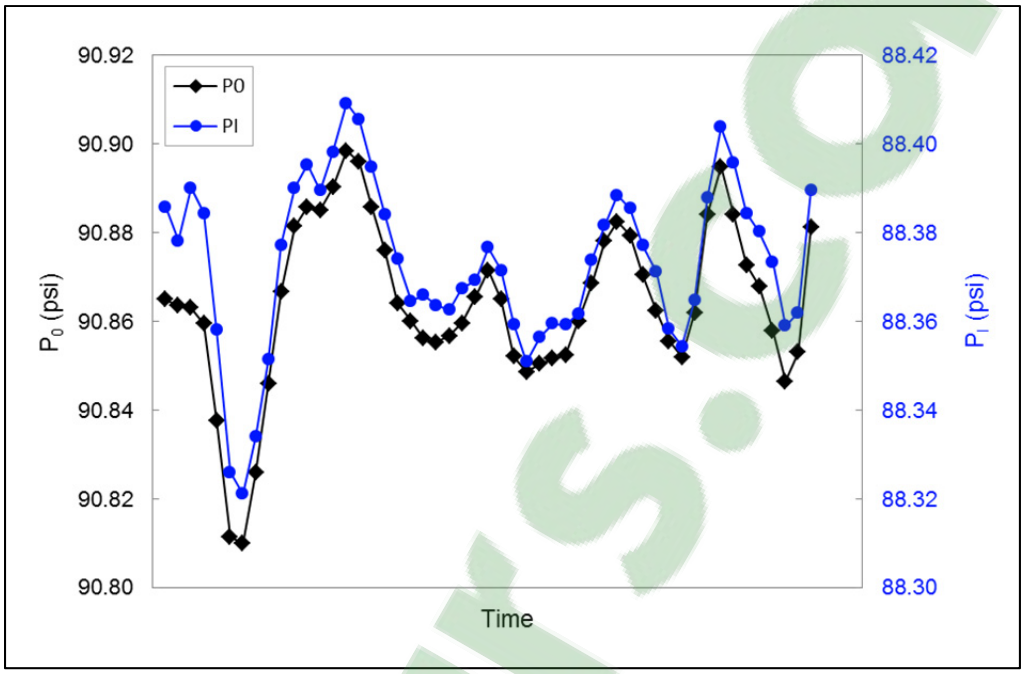

Figure 3.34 Measurements of settling chamber stagnation pressure and test section static pressure during a low speed run

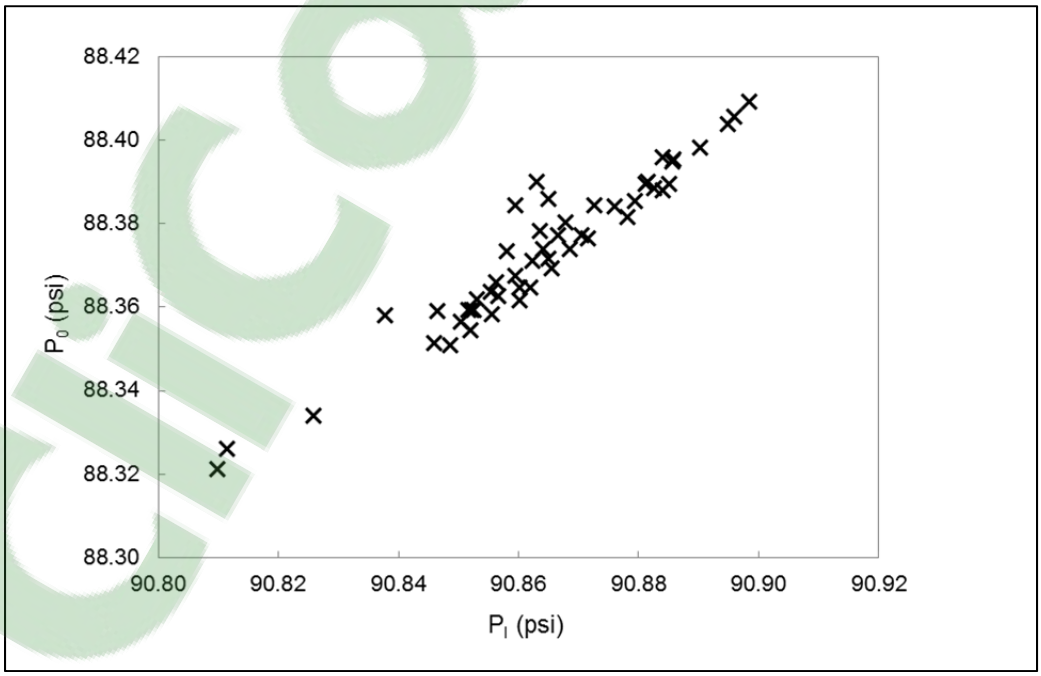

Figure 3.35 The trend in random variations of stagnation and static pressures in a low speed run

A similar analysis is carried out to compare the observed variability in the force and moment coefficients with the calculated values of their random uncertainty. However, a conventional standard deviation cannot be computed due to the lack of sufficient repeat runs. Instead, variability is estimated based on the range of the result in a set of two repeat runs. This method is typically used in statistical quality control (Montgomery, 2009) and has been implemented at the Boeing Polysonic wind tunnel (Hemsch, Hanke and Walker, 2008), as well as the NASA Langley and Glenn Research Centers (Hemsch, Hanke and Walker, 2008; Stephens et al., 2016) for assessing repeatability. The range is computed as the absolute value of the difference between the repeat values at corresponding data points, after interpolation of each result to an average angle of attack between the two runs. For each pair of repeat runs, the average range $\overline{R}$ over all angles of attack is then used to estimate the standard deviation as follows (Hemsch, Hanke and Walker, 2008)

$$\sigma = 0.8865\,\overline{R} \tag{3.6}$$

Once σ is obtained, the expanded 95-percent observed variability or 2σ can be compared with the calculated random uncertainty, averaged over the entire angle of attack range. The constant of Eq. (3.6) is taken from a table of statistical estimation factors for obtaining a standard deviation based on the range of a number of readings in a small sample, commonly used to construct the control limits of statistical quality control charts (Montgomery, 2009; Stephens et al., 2016). The factors are tabulated as a function of the sample size, and 0.8865 corresponds to a sample of two readings, as the measurements of two repeat runs are studied in the present analysis. Figures 3.36 and 3.37 provide an example of the range and the random uncertainty of the coefficient of drag for a pair of high speed runs analyzed in the validation process.

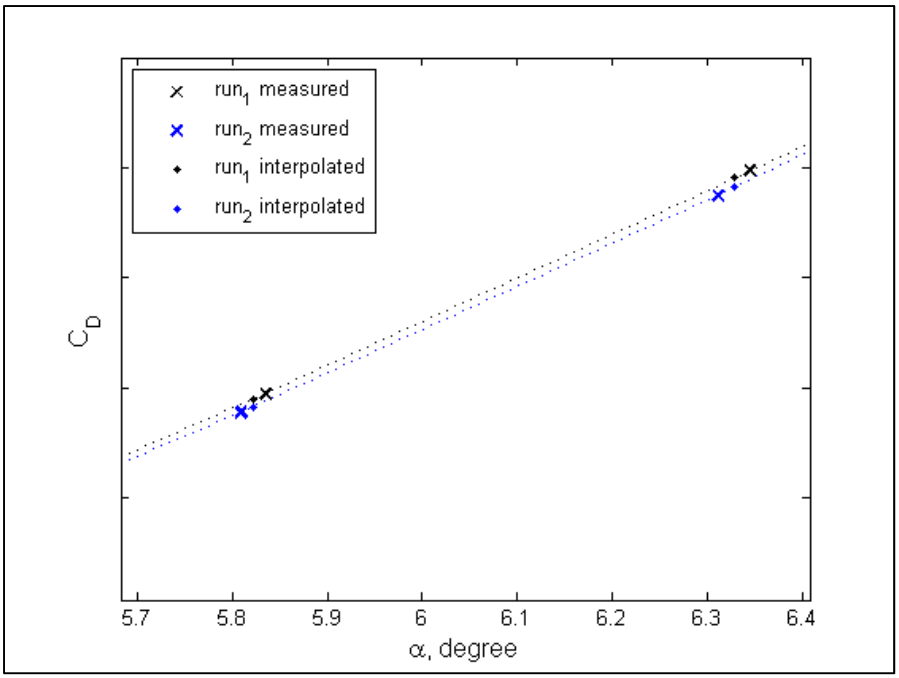

Figure 3.36 Coefficients of drag of a pair of high speed repeat runs (C_D scale = 0.005)

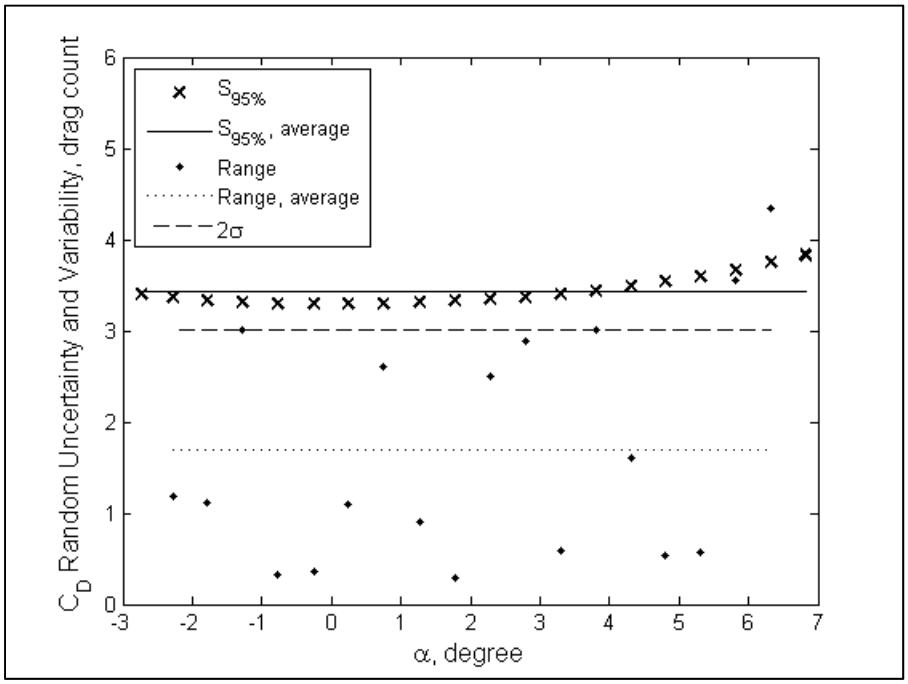

Figure 3.37 Random uncertainty and variability in drag coefficients of a pair of high speed repeat runs

As seen in Figure 3.36, C_D measurements of the two runs are first interpolated to the average angle of attack for every pair of corresponding points. The range is then calculated as the absolute value of the difference between the interpolated values, and shown in Figure 3.37 along with $S_{95\%}$, the average 95-percent random uncertainty of the two coefficients of drag. The 2σ variability of the given pair of repeat runs is estimated based on the average range according to Eq. (3.6), and compared with the average calculated random uncertainty over all the angles of attack to validate the uncertainty analysis results. The comparison is presented in Figure 3.38 and Figure 3.39 for C_D and C_L using one pair of repeat runs at every nominal operating condition, analyzed over similar angles of attack.

At high speed conditions where accurate prediction of the coefficient of drag is more important, the calculated random uncertainty and observed variability of C_D agree within one drag count which is considered satisfactory. The higher discrepancy at the low speed condition however can be a sign of undetected correlation in random errors of pressure measurements due to tunnel operation factors, as explained earlier. Since the pressure levels are higher at the low speed tests, the effects of such correlations are more pronounced, and not accounting for them overestimates the random uncertainty to a larger extent compared to the low pressure high speed tests.

A reasonable agreement also exists between the calculated random uncertainty of the coefficient of lift and the observed variability. It should be noted however that the range or the difference between the repeat C_L values varies considerably with angle of attack during the analyzed runs, suggesting that the average range may not be a suitable measure of variability. The calculated values of C_L random uncertainty also increase at a high rate with the angle of attack in some cases, but this fact is neglected when an average value is chosen to represent the estimated uncertainty for an entire run. Hence, the overall agreement is deemed reasonable, considering all the averaging performed for the purpose of comparison and given the fact that the analysis through which the calculated values are obtained is only limited to the data reduction process, and the errors due to the variations in the tunnel operation are not taken into account.

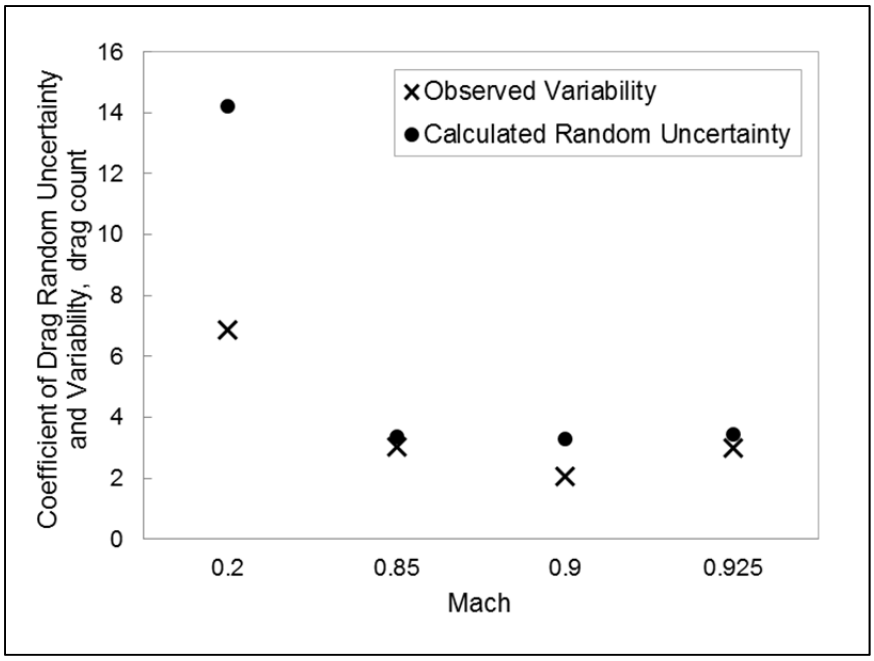

Figure 3.38 Coefficient of drag random uncertainty validation

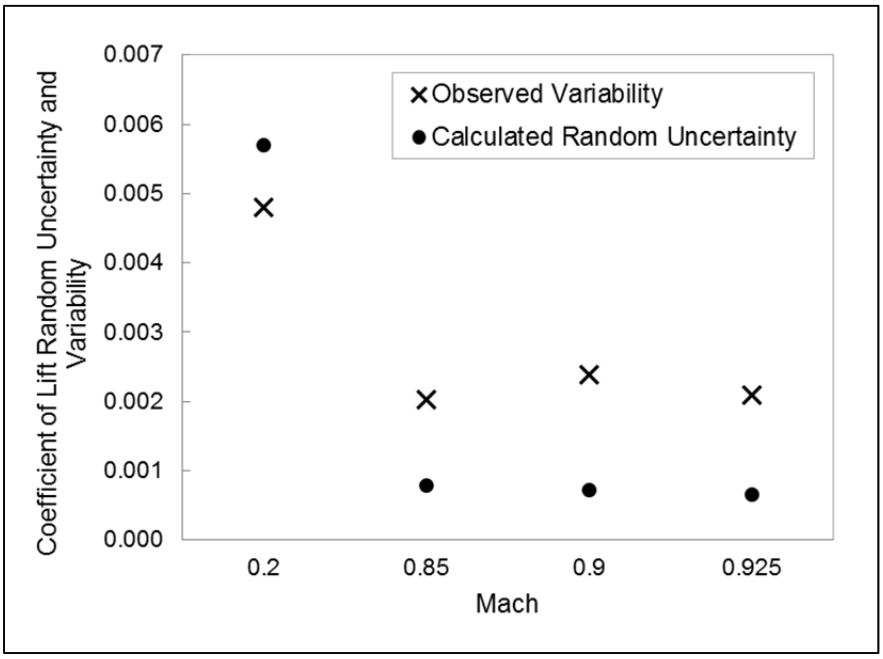

Figure 3.39 Coefficient of lift random uncertainty validation

It should be emphasized that the presented validation work on the coefficients of drag and lift is limited to a single pair of repeat runs at Mach 0.2, and a single pair at Mach 0.85 to 0.925 where three pitch sweeps were performed at three different wind speeds. More repeat tests are desired for a comprehensive validation.

CONCLUSION

With the implementation of the developed algorithm, the uncertainties in the results of the half-model experiments carried out by Bombardier Aerospace at the NRC 1.5 m trisonic wind tunnel are precisely quantified and reported at every measurement point, as part of the data reduction routine. The algorithm follows the methodology recommended by the AIAA Standard (1999) on the assessment of experimental uncertainty in wind tunnel testing. The bias and precision errors of the measured variables have been estimated from calibration data, and propagated through the data reduction equations using a Taylor series expansion to obtain the overall uncertainty of every result parameter, as a 95-percent confidence interval around the experimental value.

The analysis outcomes are reported for a number of runs, with a focus on the uncertainties of the freestream properties and the coefficients of drag and lift, under different operating conditions and for different test article configurations. The results reveal that the freestream properties are achieved with high accuracy, as the uncertainties in the freestream Mach number and dynamic pressure are respectively limited to 0.4% and 0.7% of the desired nominal values. The uncertainties in the coefficients of lift and drag vary with the operating condition, and also over the pitch sweep during a test due to functional dependence on the measured normal and axial forces, as well as the angle of attack. Since a wide range of model configurations are tested over a number of different operating conditions throughout every series of Bombardier half-model experiments, the focus of the project has been on automating the uncertainty analysis and implementing the error propagation methodology within the data reduction routine so that the uncertainties can be specified for every measurement and reported along with the test results, rather than on generalizing the overall state of data quality at the tunnel.

Detailed breakdowns of total uncertainties are obtained to separately investigate the systematic and random components, and to identify the variables that have the largest contribution to the uncertainties of the test results. The analyses reveal that an accurate

estimate of the bias errors of the measurement system is critical as the systematic uncertainties are of the same order of magnitude as the random uncertainties, commonly perceived as repeatability. Since the two add as root-sum-square to yield the total 95-percent uncertainty of the result, they deserve equal attention. Moreover, pressure and force proved to be consistently the major contributors to the uncertainties, even though the relative magnitude of their contribution varies with the tunnel operating condition and from one model configuration to another. For the particular runs presented in this thesis and with the current estimates of the precision limits, the two balance axial force components have the highest contribution to the repeatability of the drag coefficient, while that of the lift coefficient and the test section Mach number and dynamic pressure is mostly affected by the precision of the stagnation pressure measurement device. Such uncertainty breakdowns can be used to identify the areas within the measurement system that should be targeted in order to improve the overall accuracy of the experimental data most effectively. Hence, the focus of any data quality improvement initiatives can be prioritized based on the result of the uncertainty analysis.

The computational aspect of the analysis has been validated through an alternative error propagation method (Monte Carlo). The primary aspect however is the accuracy of the estimated errors of each measurement device which are propagated through the data reduction equations to yield the uncertainty of the results. It is important to verify that all the significant elemental error sources have been identified and all the correlated errors are accounted for. In the absence of sufficient repeat runs, the initial validation against observation has been done on the tunnel freestream parameters, assuming runs with nominally identical conditions can be combined to obtain an overall standard deviation to represent variability in Mach number and dynamic pressure. A satisfactory agreement exists between the observed variability in the freestream parameters and their respective estimated random uncertainty. In order to make the same comparison for the uncertainties of the force coefficients, a measure of variability based on the average range in a set of two repeat runs has been used. The average calculated random uncertainty in the repeat pairs is compared with the observed variability for the coefficients of drag and lift. Considering the effects of

all the averaging performed to compute a single representation for each metric, and given that the errors introduced by tunnel operation are inherently neglected in the adopted methodology, the agreement is rather satisfactory.

The estimated freestream Mach number and dynamic pressure total uncertainties are of the same order of magnitude as those obtained by Springer (1999) at the NASA Marshall Space Flight Center, and also by Ulbrich and Boone (2004) at the NASA Ames wind tunnel, under similar test conditions. The calculated random components of the uncertainties in these freestream parameters and how they compare to the observed measurement variability are similar to those reported at the NASA National Transonic Facility by Walter, Lawrence and Elder (2010). Consistent with the findings at the NASA Glenn (Stephens et al., 2016) and Marshall (Springer, 1999) wind tunnels, the bias errors play an important role in the overall uncertainties of Mach number and dynamic pressure at NRC. The trend in the uncertainty of the coefficient of drag with Mach number also agrees with that observed at the Marshall wind tunnel (Springer, 1999). Besides, the major contributing factors to the random uncertainty of the coefficient of drag measured at the NRC trisonic wind tunnel are similar to those identified at the Naval Surface Warfare Center hypervelocity wind tunnel (Kammeyer, 1999) and the National Trisonic Facility (Walter, Lawrence and Elder, 2010). In the present thesis and the corresponding conference paper (Fakhraei and Weiss, 2016), the uncertainty of the coefficient of lift has been analyzed over the entire angle of attack range along with its breakdown of the major contributing factors, for the first time in the literature.

The developed algorithm can benefit from a more comprehensive estimate of the bias and precision errors of the force measurements, as a detailed uncertainty analysis of the half-model strain gage force balance proved to be out of the scope of this project. The most straightforward method to obtain the bias and precision limits of the force components is through the use of calibration residuals, as recommended by the AIAA Standard (1999) and implemented at a number of wind tunnels such as the trisonic tunnel of the NASA Marshall Space Flight Center (Springer, 1999) and the hypervelocity tunnel of the Naval Surface Warfare Center (Kammeyer, 1999). The statistical theories used in deriving these limits from

the calibration residuals assume that all the errors have a Gaussian distribution. Bergmann and Philipsen (2010) advise that such an assumption be verified before adopting the methodology. A histogram of the residuals for every force component of the NRC half-model balance in the 2011 calibration and the 2014 calibration check indeed confirmed the Gaussian behavior of the errors. As expressed by Belter (1998) at the Boeing Aerodynamics Laboratory, obtaining the precision limit of the force measurements from the balance calibration residuals generally yields the most conservative estimates of repeatability. The other more involved methods of obtaining the balance uncertainty rely on the uncertainties of the curve fitting parameters of the calibration matrix or the goodness of the fit of the least-square multivariate regression (Reis, Mello and Uyeno, 2003; Reis et al., 2004; Kammeyer and Rueger, 2008; Reis, Castro and Mello, 2013). The application of these methodologies will result in balance uncertainties that depend on the readings of the strain gages during a test (Reis et al., 2002). Once better estimates of the precision and bias limits become available in the future, the uncertainty results can be easily updated and improved, since the limits are entered as inputs in the algorithm.

In the absence of sufficient repeat runs or comprehensive benchmark tests from which to directly obtain the random uncertainty of the experimental results, one can rely on the developed algorithm to quantify the overall uncertainties. However, it should be acknowledged that the employed Taylor Series Method of error propagation is limited to the data reduction process and does not take into account any variation in the result caused by the tunnel operation or the potential effects of any correlated random errors. Regardless of this inherent shortcoming, the developed uncertainty analysis algorithm is a strong tool for precisely quantifying the uncertainties in all the result parameters at every measurement point of an experiment, and also for identifying the areas within the measurement system that deserve the most attention if any data quality improvement is desired.

APPENDIX I

THE NRC TRISONIC FACILITY

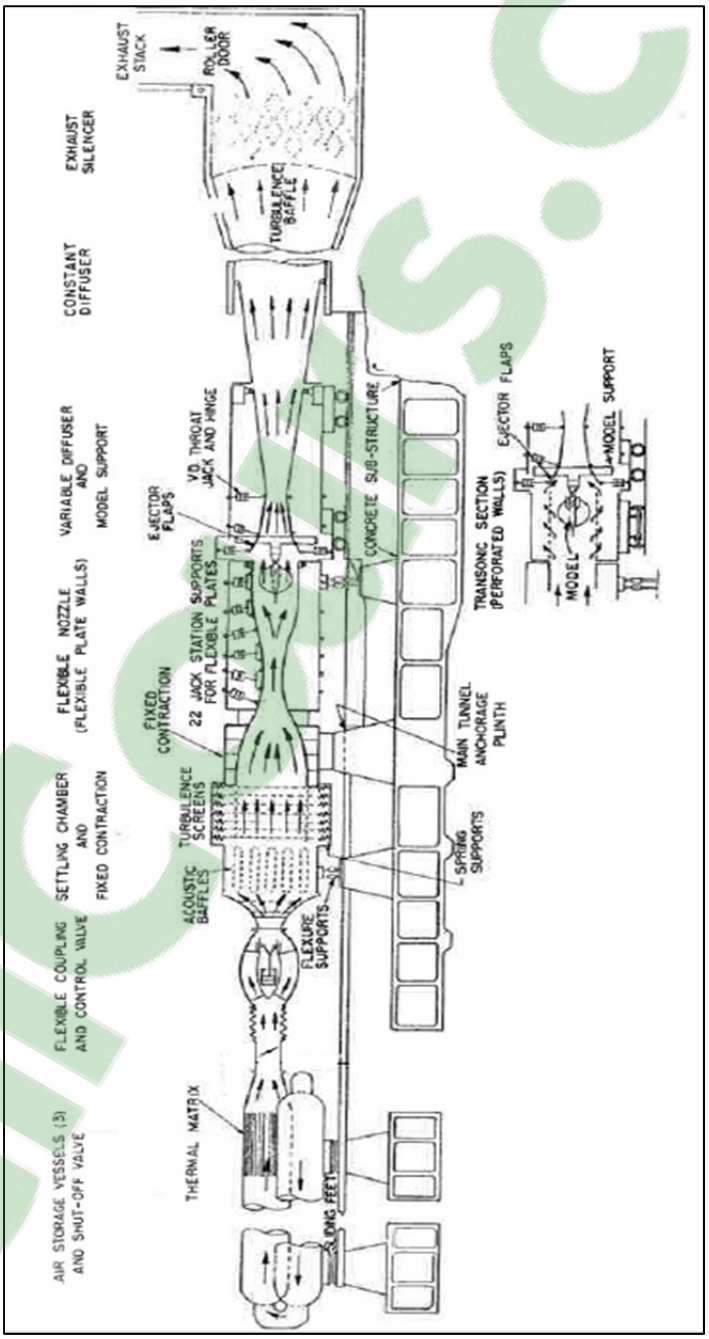

Figure-A I-1 Schematic of the NRC 1.5 m blowdown trisonic wind tunnel (taken from Brown, 1977 p. 17)

APPENDIX II

THE HALF-MODEL BALANCE

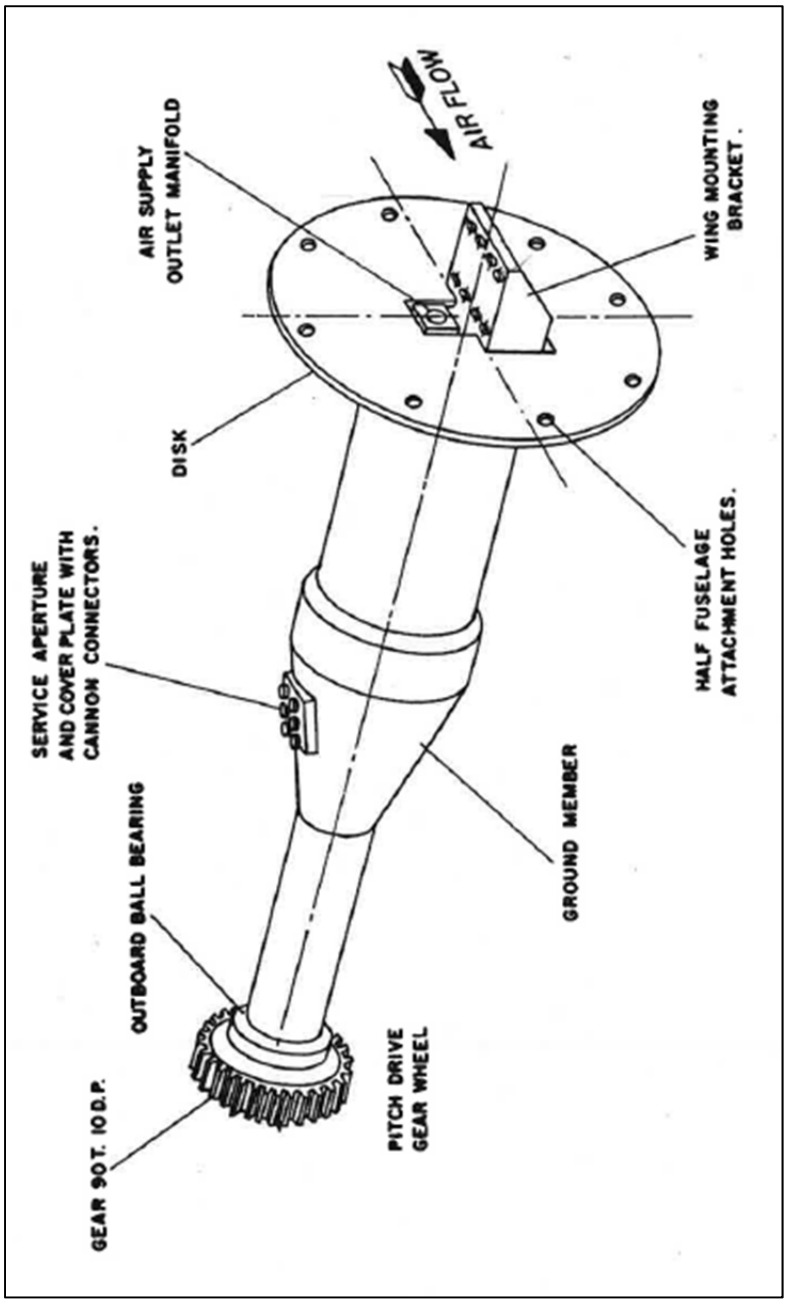

Figure-A II-1 Diagram of the half-model external strain gage force balance (taken from Orchard, 2007 p. 35)

LIST OF REFERENCES

American Institute of Aeronautics and Astronautics. 1999. *Assessment of Experimental Uncertainty with Application to Wind Tunnel Testing*. AIAA Standard, S–071A–1999. Reston, VA: American Institute of Aeronautics and Astronautics, 248 p.

Belter, Dale L. 1998. "Comparison of Wind-Tunnel Data Repeatability with Uncertainty Analysis Estimates". AIAA Paper 98-2714. Reston, VA: American Institute of Aeronautics and Astronautics.

Bergmann, R. and I. Philipsen. 2010. "Some Contemplation on a Proposed Definition of Uncertainty for Balances". In *27th AIAA Aerodynamic Measurement Technology and Ground Testing Conference*. (Chicago, Il, Jun. 28-Jul. 1 2010), AIAA Paper 2010-4546. Reston, VA: American Institute of Aeronautics and Astronautics.

Brown, D. 1977. *Information for Users of the National Research Council's 5-ft x 5-ft Blowdown Wind Tunnel at the National Aeronautical Establishment*. "Laboratory Technical Report", LTR-HA-6. Ottawa, ON: National Research Council Canada, 42 p.

Coleman, Hugh W. and W. Glenn Steele. 2009. *Experimentation and Uncertainty Analysis for Engineers*, 3rd ed. New Jersey, NY: John Wiley & Sons, 317 p.

Fakhraei, Samin and Julien Weiss. 2016. "Uncertainty Analysis of Test Data at the NRC 1.5-Meter Trisonic Wind Tunnel." In *32nd AIAA Aerodynamic Measurement Technology and Ground Testing Conference*. (Washington, DC, Jun. 13-17), AIAA-2016-3498. Reston, VA: American Institute of Aeronautics and Astronautics.

Hemsch Michaek J., Jeremy L. Hanke and Eric L.Walker. 2008. "Detailed Uncertainty Analysis for Ares I Ascent Aerodynamics Wind Tunnel Database". In *26th AIAA Aerodynamic Measurement Technology and Ground Testing Conference*. (Seattle, WA, Jun. 23-26 2008), AIAA Paper 2008-4259. Reston, VA: American Institute of Aeronautics and Astronautics.

Kammeyer, Mark E. 1999. "Uncertainty Analysis for Force Testing in Production Wind Tunnels". In *First International Symposium on Strain Gauge Balances*. (Hampton, VA, Oct. 22-25 1996), p. 221-242. Hampton, VA: National Aeronautics and Space Administration.

Kammeyer, Mark E. and Mathew L. Rueger. 2008. "Estimation of the Uncertainty in the Internal Balance Calibration through Comprehensive Error Propagation". In *26th AIAA Aerodynamic Measurement Technology and Ground Testing Conference*. (Seattle, WA, Jun. 23-26 2008), AIAA Paper 2008-4029. Reston, VA: American Institute of Aeronautics and Astronautics.

Meyn, Larry A. 2000. “An Uncertainty Propagation Methodology That Simplifies Uncertainty Analyses”. In *38th AIAA Aerospace Sciences Meeting and Exhibit*. (Reno, NV, Jan. 10-13 2000), AIAA Paper 2000-0149. Reston, VA: American Institute of Aeronautics and Astronautics.

Montgomery, Douglas C. 2009. *Introduction to Statistical Quality Control*, 6th ed. New Jersey, NY: John Wiley & Sons, 734 p.

Orchard, D. M., C. Broughton, Y. Mebarki and D. Hamilton. 2007. *Bombardier CRJ900-X Half-Model High-Lift Test in the IAR 1.5m x 1.5m Trisonic Wind Tunnel*. “Laboratory Technical Report”, LTR-AL-2007-2008. Ottawa, ON: National Research Council Canada Aerodynamics Laboratory, 51 p.

Reis, Maria L.C.C., Olympio A.F. Mello, Sadahaki Uyeno and Osvaldo S. Sampaio. 2003. “A Method for Estimation of the Calibration Uncertainty of an External Six Component Wind Tunnel Balance”. In *22nd AIAA Aerodynamic Measurement Technology and Ground Testing Conference*. (St. Louis, MO, Jun. 24-26 2002), AIAA Paper 2002-2793. Reston, VA: American Institute of Aeronautics and Astronautics.

Reis, Maria L.C.C., Olympio A.F. Mello and Sadahaki Uyeno. 2003. “Calibration Uncertainty of an External Six-Component Wind Tunnel Balance”. In *33rd AIAA Fluid Dynamics Conference and Exhibit*. (Orlando, FL, Jun. 23-26), AIAA Paper 2003-3884. Reston, VA: American Institute of Aeronautics and Astronautics.

Reis, Maria L.C.C., Wilson J. Vieira, Itamar M. Barbosa, Olympio A.F. Mello and Luciano A. Santos. 2004. “Validation of an External Six-Component Wind Tunnel Balance Calibration”. In *24th AIAA Aerodynamic Measurement Technology and Ground Testing Conference*. (Portland, OR, Jun. 28-Jul. 1 2004), AIAA Paper 2004-2300. Reston, VA: American Institute of Aeronautics and Astronautics.

Reis, M.L.C.C., R.M. Castro and O.A.F. Mello. 2013. “Calibration Uncertainty Estimation of a Strain-Gage External Balance”. *Measurement*, 46, 24-33.

Springer, Anthony M. 1999. “Uncertainty Analysis of the NASA MSFC 14-inch Trisonic Wind Tunnel”. In *37th AIAA Aerospace Sciences Meeting and Exhibit*. (Reno, NV, Jan. 11-14 1999), AIAA Paper 99-0684. Reston, VA: American Institute of Aeronautics and Astronautics.

Stephens, Julia E., Erin P. Hubbard, Joel A. Walter and Tyler McElroy. 2016. “Uncertainty Analysis of NASA Glenn’s 8- by 6-foot Supersonic Wind Tunnel”. In *54th AIAA Aerospace Sciences Meeting*. (San Diego, CA, Jan 4-8 2016), AIAA Paper 2016-1148. Reston, VA: American Institute of Aeronautics and Astronautics.

Ulbrich, N. and A. R. Boone. 2004. “Uncertainty Analysis of Test Data in the Ames 11-Foot Transonic Wind Tunnel”. In *24th AIAA Aerodynamic Measurement Technology and Ground Testing Conference*. (Portland, OR, Jun. 28-Jul. 1 2004), AIAA Paper 2004-2195. Reston, VA: American Institute of Aeronautics and Astronautics.

Walter, Joel A., William R. Lawrence and David W. Elder. 2010. “Development of an Uncertainty Model for the National Transonic Facility”. In *27th AIAA Aerodynamic Measurement Technology and Ground Testing Conference*. (Chicago, IL, Jun. 28-Jul. 1 2010), AIAA Paper 2010-4925. Reston, VA: American Institute of Aeronautics and Astronautics.